

# Solving eigenvalue PDEs of metastable diffusion processes using artificial neural networks

Wei Zhang <sup>\*</sup>    Tiejun Li <sup>†</sup>    Christof Schütte <sup>‡</sup>

## Abstract

In this paper, we consider the eigenvalue PDE problem of the infinitesimal generators of metastable diffusion processes. We propose a numerical algorithm based on training artificial neural networks for solving the leading eigenvalues and eigenfunctions of such high-dimensional eigenvalue problem. The algorithm is able to find multiple leading eigenpairs by solving a single training task. It is useful in understanding the dynamical behaviors of metastable processes on large timescales. We demonstrate the capability of our algorithm on a high-dimensional model problem, and on the simple molecular system alanine dipeptide.

**Keywords**— eigenvalue PDE, metastable process, molecular dynamics, artificial neural network, variational characterization

## 1 Introduction

Understanding the dynamics of molecular systems is often a challenging task due to the high dimensionality of the systems and their extraordinarily complex dynamical behavior. In the last decades, considerable amount of efforts have been devoted to developing high-performance numerical packages and new simulation techniques, leading to the rapid advance of the capability of molecular dynamics simulations in generating trajectory data. At the same time, many data-based numerical approaches have emerged, which allow to efficiently study the molecular kinetics through analyzing the trajectory data obtained from molecular dynamics simulations. A large class of these approaches for trajectory data analysis are based on the theory of

---

<sup>\*</sup>Zuse Institute Berlin, Takustrasse 7, 14195 Berlin, Germany. Email: wei.zhang@fu-berlin.de

<sup>†</sup>Laboratory of Mathematics and Applied Mathematics (LMAM) and School of Mathematical Sciences, Peking University, Beijing 100871. P.R. China. Email: tieli@pku.edu.cn

<sup>‡</sup>Institut für Mathematik, Freie Universität Berlin and Zuse Institute Berlin, D-14195 Berlin, Germany; christof.schuette@fu-berlin.de

the transfer operator [61] or Koopman operator [5], hence termed operator-based approaches, in which the molecular system is analyzed by estimating the dominant eigenvalues and their corresponding eigenfunctions of the operator that is discretized using trajectory data. Notable examples are the variational approach to conformational dynamics [44, 45] and its linear version, time lagged independent component analysis (tICA) [50], the variational approach for Markov processes (VAMP) [69], the extended dynamic mode decompositions [68, 27, 28], Markov state models (MSMs) [55, 9, 23], etc. Recent development in these directions includes the kernel-tICA [62] using kernel method, the deep learning frameworks VAMPNets [40] and the state-free reversible VAMPNets (SRVs) [7] for molecular kinetics.

In contrast to the transfer operator and the Koopman operator, the infinitesimal generator (henceforth called generator) is a key operator of a molecular system that does not rely on the choice of the lag time. Similar to the aforementioned operator-based approaches using the transfer operator or the Koopman operator, crucial information on the underlying dynamics can be obtained by analyzing the system’s generator as well. For instance, the leading eigenvalues of the generator encode the dominant timescales of metastable molecular systems, whereas the corresponding eigenfunctions are in fact good collective variables for constructing low-dimensional coarse-grained dynamics [71]. In a broader context, many probabilistic quantities of a Markov process can be represented as the solution to certain partial differential equation (PDE) that involves the system’s generator [47, 34]. This fact has inspired the PDE-based approaches, which have been successfully applied in analyzing various aspects of Markov processes, such as metastability [3, 4], transition paths [67], and more recently the model reduction of molecular dynamics [71]. Moreover, data-based methods for estimating the eigenvalues and eigenfunctions of the generator are available [72].

The overdamped Langevin dynamics [47, 49] is often adopted in modelling molecular dynamics in equilibrium due to its simplicity and nice properties for mathematical analysis. In this context, we consider a smooth potential function  $V : \mathbb{R}^d \rightarrow \mathbb{R}$  in state space  $\mathbb{R}^d$ , a matrix-valued function  $\sigma : \mathbb{R}^d \rightarrow \mathbb{R}^{d \times d_1}$ , where  $d, d_1$  are two integers such that  $1 \leq d \leq d_1$ , and we define the function  $a : \mathbb{R}^d \rightarrow \mathbb{R}^{d \times d}$  by  $a = \sigma \sigma^T$ . The entries of the matrix  $a(x)$  at  $x \in \mathbb{R}^d$  are  $a_{ij}(x)$ , where  $1 \leq i, j \leq d$ . Then, the overdamped Langevin dynamics is described by the stochastic differential equation (SDE)

$$dx(s) = -a(x(s))\nabla V(x(s)) ds + \frac{1}{\beta}(\nabla \cdot a)(x(s)) ds + \sqrt{2\beta^{-1}}\sigma(x(s)) dw(s) \quad (1)$$

where  $x(s) \in \mathbb{R}^d$  is the state of the system at time  $s \in [0, +\infty)$ ,  $\beta > 0$  is a constant proportional to the inverse of the system’s temperature,  $(w(s))_{s \geq 0}$  is a Brownian motion in  $\mathbb{R}^{d_1}$ , and  $\nabla \cdot a : \mathbb{R}^d \rightarrow \mathbb{R}^d$  denotes the vector-valued function whose components are given by  $(\nabla \cdot a)_i(x) = \sum_{j=1}^d \frac{\partial a_{ij}}{\partial x_j}(x)$

for  $i = 1, \dots, d$  and for all  $x \in \mathbb{R}^d$ . The reason for including the term  $\frac{1}{\beta} \nabla \cdot a$  in (1) is to make sure that under certain assumptions (see Section 2.1) the process (1) is ergodic with respect to the unique invariant probability distribution  $\mu$ , defined by

$$\mu(dx) = \frac{1}{Z} e^{-\beta V(x)} dx, \quad x \in \mathbb{R}^d, \quad (2)$$

where  $Z = \int_{\mathbb{R}^d} e^{-\beta V(x)} dx$  is the normalizing constant. We refer to [12, Section 5], [43, Theorem 5.3], and [13, Theorem 1] for sufficient conditions on ergodicity and to [47, 49] for a more detailed introduction to the SDE (1).

The main focus of this paper is the eigenvalue problem defined by the (high-dimensional) PDE

$$-\mathcal{L}\varphi = \lambda\varphi, \quad \text{in } \mathbb{R}^d \quad (3)$$

associated to the generator  $\mathcal{L}$  of SDE (1), given by

$$\mathcal{L}f = \frac{e^{\beta V}}{\beta} \sum_{i,j=1}^d \frac{\partial}{\partial x_j} \left( e^{-\beta V} a_{ij} \frac{\partial f}{\partial x_i} \right), \quad (4)$$

where  $f : \mathbb{R}^d \rightarrow \mathbb{R}$  is a test function. In particular, when  $a$  is the identity matrix of size  $d$ , the generator  $\mathcal{L}$  in (4) has the well-known form

$$\mathcal{L}f = -\nabla V \cdot \nabla f + \frac{1}{\beta} \Delta f. \quad (5)$$

Under mild conditions (see Section 2.1), the operator  $\mathcal{L}$  is self-adjoint with respect to a weighted inner product and it has purely discrete spectrum. Moreover, one can show that the eigenvalues of the problem (3) are all positive real numbers, except the trivial one  $\lambda_0 = 0$  whose corresponding eigenfunction is  $\varphi_0 \equiv 1$ . In this paper, we are interested in computing the first non-trivial  $K$  eigenvalues (in non-decreasing order) and the corresponding eigenfunctions of (3) for some integer  $K \geq 1$ , i.e., the eigenpairs  $\{(\lambda_i, \varphi_i)\}_{1 \leq i \leq K}$ , where

$$0 = \lambda_0 < \lambda_1 \leq \lambda_2 \leq \dots \leq \lambda_K \leq \dots \quad (6)$$

Given  $K \geq 1$ , the main contribution of this paper is a novel numerical method for computing the eigenpairs  $\{(\lambda_i, \varphi_i)\}_{1 \leq i \leq K}$  of (3) by training artificial neural networks. Designing the loss function based on certain variational formulation of the eigenpairs of (3), we propose a training task which computes multiple eigenpairs of the problem (3) at once. The method can be applied to solving high-dimensional eigenvalue PDEs (i.e.,  $d$  is large) where the operator  $\mathcal{L}$  is of the general form (4). To overcome the metastability in sampling the training data according to  $\mu$ , a reweighting technique

is proposed, which allows the use of biased training data sampled from a distribution other than  $\mu$ .

In the following let us mention several existing work on related topics and discuss the novelty of the current work. Firstly, the aforementioned numerical approaches based on the transfer operator or the Koopman operator (see the discussion at the beginning of this introduction) require a careful choice of the lag time [55]. In contrast, our method based on the generator does not involve the lag time. The current work extends the data-based method using basis functions in [72] to the neural network framework. As a result, the algorithm in this work does not require the choice of basis functions, and therefore is suitable for solving high-dimensional problems. We note that similar biased sampling and reweighting technique have been employed in [2, 37]. Secondly, beyond the study of dynamical systems, there has been growing research interest in recent years in developing deep learning-based numerical methods for solving high-dimensional PDEs, such as parabolic PDEs [17], the committor equation (a boundary value elliptic PDE) in molecular dynamics [37], and the eigenvalue PDEs [14, 18]. We also refer to the recent work [39, 19, 21, 53] for deep learning-based methods for solving eigenvalue problems in quantum physics. In contrast to these existing methods for eigenvalue PDEs which typically compute the first eigenvalue of the problem, our algorithm is able to find multiple eigenpairs by solving a single training task. Lastly, we note that finding good low-dimensional collective variables for complex molecular systems is of great importance in the study of molecular kinetics. Various approaches are proposed, using for instance the eigenfunctions in the operator-based approaches [50], feature engineering [51, 64, 65], and autoencoders [8, 6, 63, 2]. Although this topic is not the focus of the current paper, we point out that it is potentially possible to reformulate our (training) algorithm as an algorithm for finding good collective variables of molecular systems. The application of the current work in this direction will be explored in future work.

The remainder of this article is organized as follows. In Section 2, we present the mathematical setting of the eigenvalue PDE problem considered in this paper, and in particular we study its variational formulations. In Section 3, we present the numerical algorithm for solving the eigenvalue PDE problem by training artificial neural networks. In Section 4, we demonstrate our algorithm by studying two numerical examples. In Section 5, we conclude with discussions on various issues. Appendix A contains the proofs of two results in Section 2.

## 2 Mathematical setting

In this section we present mathematical background of the eigenvalue problem (3). In particular, we provide variational formulations for the lead-

ing eigenpairs of the eigenvalue problem (3).

## 2.1 Preliminary

Throughout this paper, we make the following assumption on the function  $a$  in (4).

**Assumption 1.** *The function  $a : \mathbb{R}^d \rightarrow \mathbb{R}^{d \times d}$  is  $C^2$ -smooth and satisfies the (uniform ellipticity) condition*

$$v^T a(x) v \geq a^- |v|^2, \quad \forall x, v \in \mathbb{R}^d, \quad (7)$$

for some positive constant  $a^- > 0$ .

We denote by  $\mathbb{N} := \{1, 2, \dots\}$  the set of natural numbers. The mean value of a measurable function  $f : \mathbb{R}^d \rightarrow \mathbb{R}$  with respect to the invariant probability measure  $\mu$  defined in (2) is denoted as  $\mathbf{E}_\mu(f)$  provided that it exists, i.e.,

$$\mathbf{E}_\mu(f) := \int_{\mathbb{R}^d} f(x) \mu(dx). \quad (8)$$

The Hilbert space  $L^2(\mu)$  consists of all measurable functions that are square-integrable with respect to  $\mu$ , with the norm and the inner product defined by, respectively,

$$\|f\|_\mu := \mathbf{E}_\mu(f^2)^{\frac{1}{2}}, \quad \langle f, g \rangle_\mu := \mathbf{E}_\mu(fg), \quad \forall f, g \in L^2(\mu). \quad (9)$$

Also recall the following expressions of the variance and the covariance of functions with respect to  $\mu$  : for  $f, g \in L^2(\mu)$ ,

$$\text{var}_\mu(f) = \mathbf{E}_\mu(f^2) - (\mathbf{E}_\mu(f))^2, \quad \text{cov}_\mu(f, g) = \mathbf{E}_\mu(fg) - \mathbf{E}_\mu(f)\mathbf{E}_\mu(g). \quad (10)$$

Clearly, we have  $\text{cov}_\mu(f, f) = \text{var}_\mu(f)$  for all  $f \in L^2(\mu)$ . For the operator  $\mathcal{L}$  (4), using (2) and the integration by parts formula, we can verify that

$$\langle (-\mathcal{L})f, g \rangle_\mu = \langle f, (-\mathcal{L})g \rangle_\mu = \frac{1}{\beta} \mathbf{E}_\mu((a \nabla f) \cdot \nabla g), \quad (11)$$

for all  $C^2$  test functions  $f, g$  such that the integrals in (11) are well-defined.

In the following we collect some useful results from [13]. We need the following assumption [13, Assumptions B and C] on  $V$ .

**Assumption 2.** *The function  $V \in C^2(\mathbb{R}^d)$  is bounded from below and satisfies:*

1. *There exists  $\delta \in (0, 1)$ , such that*

$$\liminf_{|x| \rightarrow +\infty} ((1 - \delta)\beta |\nabla V(x)|^2 - \Delta V(x)) > 0; \quad (12)$$

$$2. \lim_{|x| \rightarrow +\infty} |\nabla V(x)| = +\infty.$$

Define the space  $L_0^2(\mu) := \{f \in L^2(\mu) \mid \mathbf{E}_\mu(f) = 0\}$ . Under Assumptions 1–2, using (11) and the inequality (16) in Lemma 1 below we can show that  $\|\cdot\|_1$ , given by

$$\|f\|_1 := \langle f, (-\mathcal{L})f \rangle_\mu^{\frac{1}{2}} \quad (13)$$

for a test function  $f$ , defines a norm in the space

$$\mathcal{H}^1 := \left\{ f \in L^2(\mu) \mid \mathbf{E}_\mu(f) = 0, \|f\|_1 < +\infty \right\} \quad (14)$$

and it satisfies the Pythagorean identity. Therefore, the completion of  $\mathcal{H}^1$  with respect to  $\|\cdot\|_1$  (13) is a Hilbert space, which we again denote by  $\mathcal{H}^1$ . The inner product  $\langle f, g \rangle_1$  of  $\mathcal{H}^1$ , defined through polarization, is actually given by (11) for all test functions  $f, g \in \mathcal{H}^1$ . A detailed analysis of the space  $\mathcal{H}^1$  can be found in [48].

In view of the last expression in (11), we define the energy  $\mathcal{E} : L_0^2(\mu) \rightarrow [0, +\infty]$  as

$$\mathcal{E}(f) := \begin{cases} \frac{1}{\beta} \mathbf{E}_\mu((a\nabla f) \cdot \nabla f), & f \in \mathcal{H}^1, \\ +\infty & f \in L_0^2(\mu) \setminus \mathcal{H}^1. \end{cases} \quad (15)$$

The operator  $\mathcal{L}$  can be extended to a self-adjoint operator on  $L_0^2(\mu)$ , with the domain  $D(\mathcal{L}) = \{\psi \in L_0^2(\mu) \mid \exists f \in L_0^2(\mu), \mathcal{L}\psi = f\}$ . By Cauchy-Schwarz inequality, it is straightforward to verify that  $\|\psi\|_1 < +\infty$  for all  $\psi \in D(\mathcal{L})$ , from which we conclude that  $D(\mathcal{L}) \subset \mathcal{H}^1$ .

Assumptions 1 and 2 are sufficient to guarantee the compactness of the embedding  $\mathcal{H}^1 \hookrightarrow L_0^2(\mu)$ , as stated in Lemma 1 below.

**Lemma 1** ([13, Lemma 2]). *Suppose that Assumptions 1 and 2 hold. Then the embedding  $\mathcal{H}^1 \hookrightarrow L_0^2(\mu)$  is compact. The operator  $\mathcal{L}$  satisfies the Poincaré inequality:*

$$\lambda \|g\|_\mu^2 \leq \langle g, (-\mathcal{L})g \rangle_\mu, \quad \forall g \in \mathcal{H}^1, \quad (16)$$

where  $\lambda$  is a positive constant. Moreover, for all  $f \in L_0^2(\mu)$ , there exists a unique  $\psi \in \mathcal{H}^1$  such that  $-\mathcal{L}\psi = f$ .

Note that Lemma 1 implies that the operator  $-\mathcal{L} : D(\mathcal{L}) \rightarrow L_0^2(\mu)$  is bijective and therefore admits a unique inverse  $(-\mathcal{L})^{-1}$ .

In the following we consider the spectrum of  $-\mathcal{L}$ . We show that  $-\mathcal{L}$  has purely discrete spectrum under Assumptions 1 and 2. Let us first recall some definitions. Denote by  $I$  the identity operator on  $L_0^2(\mu)$ . The spectrum of  $-\mathcal{L}$ , denoted by  $\sigma(-\mathcal{L})$ , is the set consisting of all complex values  $\lambda \in \mathbb{C}$ , for which the operator  $-\mathcal{L} - \lambda I : D(-\mathcal{L}) \subset L_0^2(\mu) \rightarrow L_0^2(\mu)$  does not have a bounded inverse. The self-adjointness of  $-\mathcal{L}$  implies that  $\sigma(-\mathcal{L}) \subset \mathbb{R}$ .

In this case, the discrete spectrum of  $-\mathcal{L}$ , denoted by  $\sigma_{disc}(-\mathcal{L})$ , is the subset of  $\sigma(-\mathcal{L})$  consisting of isolated eigenvalues  $\lambda \in \sigma(-\mathcal{L})$  with finite multiplicity, i.e.,  $\{\lambda' \in \mathbb{C} \mid \lambda' \in \sigma(-\mathcal{L}), |\lambda' - \lambda| < \epsilon\} = \{\lambda\}$  for some  $\epsilon > 0$  and the eigenspace  $\{\psi \in L_0^2(\mu) \mid -\mathcal{L}\psi = \lambda\psi\}$  has finite (non-zero) dimension. We say that  $-\mathcal{L}$  has purely discrete spectrum if  $\sigma(-\mathcal{L}) = \sigma_{disc}(-\mathcal{L})$ . See [66, Section 2.4] and [58, Chapter VII and Section VIII.3] for careful studies on the spectrum of self-adjoint operators in Hilbert spaces.

Applying Lemma 1, we obtain the results below which guarantee the compactness of  $(-\mathcal{L})^{-1}$  and the fact that  $-\mathcal{L}$  has purely discrete spectrum. Its proof is presented in Appendix A.

**Proposition 1.** *The following two results hold under Assumptions 1 and 2.*

1. *The operator  $(-\mathcal{L})^{-1} : L_0^2(\mu) \rightarrow L_0^2(\mu)$  is compact.*
2. *There exist an orthonormal basis  $(\varphi_i)_{i \geq 1}$  in  $D(\mathcal{L})$  and a sequence of positive numbers  $(\lambda_i)_{i \geq 1}$ , where  $0 < \lambda_1 \leq \lambda_2 \leq \dots$  and  $\lim_{i \rightarrow +\infty} \lambda_i = +\infty$ , such that  $-\mathcal{L}\varphi_i = \lambda_i\varphi_i$  for  $i \geq 1$ . Moreover, we have*

$$\sigma(-\mathcal{L}) = \sigma_{disc}(-\mathcal{L}) = \{\lambda_1, \lambda_2, \lambda_3, \dots\}. \quad (17)$$

## 2.2 Variational characterization

In this section, we present a variational characterization of the first  $K$  eigenpairs  $\{(\lambda_i, \varphi_i)\}_{1 \leq i \leq K}$  of (3), where  $K \in \mathbb{N}$ . Note that by Proposition 1 we can assume without loss of generality that the eigenfunctions  $(\varphi_i)_{1 \leq i \leq K}$  are both normalized and pairwise orthogonal.

First, let us recall the min-max theorem for positive definite operators [38, Section 12.1], i.e.,

$$\lambda_k = \min_{H_k} \max_{f \in H_k, \|f\|_\mu = 1} \mathcal{E}(f), \quad k \geq 1, \quad (18)$$

where  $\lambda_k$  is the  $k$ th eigenvalue of (3) in (6),  $\mathcal{E}(\cdot)$  is the energy in (15), and the minimum is over all  $k$ -dimensional subspaces  $H_k$  of  $\mathcal{H}^1$ . In particular, (18) with  $k = 1$  implies that the first eigenpair  $(\lambda_1, \varphi_1)$  solves

$$\lambda_1 = \mathcal{E}(\varphi_1), \quad \text{where } \varphi_1 \in \arg \min_{f \in \mathcal{H}^1, \|f\|_\mu = 1} \mathcal{E}(f). \quad (19)$$

To present the variational characterization of the first  $K$  eigenpairs, let us define the matrix for  $k \in \mathbb{N}$

$$F^{(k)}(f_1, f_2, \dots, f_k) = \left( F_{jj'}^{(k)}(f_1, f_2, \dots, f_k) \right)_{1 \leq j, j' \leq k} \in \mathbb{R}^{k \times k}, \quad (20)$$

$$\text{where } F_{jj'}^{(k)}(f_1, f_2, \dots, f_k) = \frac{1}{\beta} \int_{\mathbb{R}^d} (a \nabla f_j) \cdot \nabla f_{j'} \, d\mu,$$

for functions  $f_1, f_2, \dots, f_k \in \mathcal{H}^1$ . The main result of this section is then the following variational characterization of the first  $K$  eigenpairs  $\{(\lambda_i, \varphi_i)\}_{1 \leq i \leq K}$ .

**Theorem 1.** *Let  $K \in \mathbb{N}$ . Suppose that Assumptions 1 and 2 hold. Define the diagonal matrix*

$$\Sigma := \text{diag}\{\omega_1, \omega_2, \dots, \omega_K\} \in \mathbb{R}^{K \times K}, \quad (21)$$

where  $(\omega_i)_{1 \leq i \leq K}$  is a non-increasing sequence of positive numbers, i.e.,  $\omega_1 \geq \dots \geq \omega_K > 0$ . Then, we have

$$\sum_{i=1}^K \omega_i \lambda_i = \min_{f_1, \dots, f_K \in \mathcal{H}^1} \sum_{i=1}^K \omega_i \mathcal{E}(f_i) = \min_{f_1, \dots, f_K \in \mathcal{H}^1} \text{tr} \left( \Sigma F^{(K)}(f_1, f_2, \dots, f_K) \right), \quad (22)$$

where  $F^{(K)}(f_1, f_2, \dots, f_K)$  is the  $K \times K$  matrix defined in (20) (with  $k = K$ ), and the minimum is over all  $f_1, f_2, \dots, f_K \in \mathcal{H}^1$  such that

$$\langle f_i, f_j \rangle_\mu = \delta_{ij}, \quad \forall i, j \in \{1, \dots, K\}. \quad (23)$$

Moreover, the minimum in (22) is achieved when  $f_i = \varphi_i$  for  $1 \leq i \leq K$ .

Theorem 1 was obtained in [72] using calculus of variations. In Appendix A, we present an alternative proof of Theorem 1 by applying Ruhe's trace inequality [60, 42].

Note that (22) reduces to the min-max theorem (19) when  $K = 1$ . In the general case, the characterization (22)-(23) allows us to develop numerical methods for computing multiple eigenpairs of  $-\mathcal{L}$  by solving a single optimization problem (see Section 3).

We conclude this section with a remark on other types of variational formulations.

**Remark 1.** *Denote by  $\lambda_{\max}(F^{(k)}(f_1, f_2, \dots, f_k))$  the maximum eigenvalue of the matrix  $F^{(k)}(f_1, f_2, \dots, f_k) \in \mathbb{R}^{k \times k}$  in (20), where  $k \in \mathbb{N}$ . By considering an orthonormal basis and applying the min-max principle for symmetric matrices to  $\lambda_{\max}(F^{(k)}(f_1, f_2, \dots, f_k))$ , we can obtain the following equivalent formulation of (18):*

$$\begin{aligned} \lambda_k &= \min_{f_1, f_2, \dots, f_k \in \mathcal{H}^1} \max_{c \in \mathbb{R}^k, |c|=1} \mathcal{E} \left( \sum_{i=1}^k c_i f_i \right) \\ &= \min_{f_1, f_2, \dots, f_k \in \mathcal{H}^1} \lambda_{\max} \left( F^{(k)}(f_1, f_2, \dots, f_k) \right), \end{aligned} \quad (24)$$

where the minimum is over all  $(f_i)_{1 \leq i \leq k} \subset \mathcal{H}^1$  such that  $\langle f_i, f_j \rangle_\mu = \delta_{ij}$  for all  $i, j \in \{1, \dots, k\}$ . Besides, the eigenvalues satisfy the max-min principle [38, Section 12.1]:

$$\lambda_k = \max_{f_1, f_2, \dots, f_{k-1} \in \mathcal{H}^1} \min_{f \in H_{k-1}^\perp, \|f\|_\mu=1} \mathcal{E}(f), \quad \forall k \geq 1, \quad (25)$$



where  $H_0^\perp = \mathcal{H}^1$  and, for fixed  $(f_i)_{1 \leq i \leq k-1} \in \mathcal{H}^1$  with  $k > 1$ ,  $H_{k-1}^\perp := \{f \in \mathcal{H}^1 \mid \langle f, f_i \rangle_\mu = 0, \forall 1 \leq i \leq k-1\}$ . Note that, in contrast to (24), in (25) the functions  $(f_j)_{1 \leq j \leq i-1}$  do not have to be linearly independent. Also, both (24) and (25) recover (19) when  $k = 1$ .

While in this paper we propose numerical algorithms based on the variational formulation (22)–(23), let us point out that it is also possible to develop numerical algorithms for computing the eigenpairs of  $-\mathcal{L}$  based on (24) or (25).

### 2.3 Neural network spaces

In this section we introduce the neural network spaces. For brevity we only consider feedforward neural networks following [52]. However, we point out that both the discussion and the numerical algorithm in this paper, i.e., Algorithm 1 in Section 3, can be directly adapted to more general types of neural networks.

Given  $L, N_0, N_1, \dots, N_L \in \mathbb{N}$ , the space  $\mathcal{S}$  of  $L$ -layer neural networks with the architecture

$$\mathcal{N} := (N_0, N_1, \dots, N_L) \quad (26)$$

is defined as the set of sequences of matrix-vector tuples

$$\mathcal{S} := \left\{ \left( (A_\ell, b_\ell) \right)_{1 \leq \ell \leq L} \mid A_\ell \in \mathbb{R}^{N_\ell \times N_{\ell-1}}, b_\ell \in \mathbb{R}^{N_\ell}, \ell \in \{1, 2, \dots, L\} \right\}. \quad (27)$$

For each  $\Phi \in \mathcal{S}$ , there are  $N_\ell$  neurons in the  $\ell$ th layer of  $\Phi$ , where  $\ell \in \{0, 1, \dots, L\}$ . These layers are called the input layer for  $\ell = 0$ , the output layer for  $\ell = L$ , and the hidden layer for  $1 \leq \ell < L$ , respectively. See Figure 1 for the illustration of neural networks with  $L = 4$  layers. Note that the space  $\mathcal{S}$  can be viewed as the Euclidean space  $\mathbb{R}^N$ , where the dimension  $N = \sum_{\ell=1}^L N_\ell(N_{\ell-1} + 1)$  is equal to the total number of parameters in a neural network  $\Phi \in \mathcal{S}$ .

Next, we discuss the use of neural networks in representing functions. Let  $\rho : \mathbb{R} \rightarrow \mathbb{R}$  be a  $C^1$ -smooth activation function. Given a neural network  $\Phi = ((A_\ell, b_\ell))_{1 \leq \ell \leq L} \in \mathcal{S}$  with the architecture  $\mathcal{N}$  (26), the realization of  $\Phi$  is defined as the function  $\mathcal{R}(\Phi) := f \in C(\mathbb{R}^{N_0}, \mathbb{R}^{N_L})$ , whose value  $f(x) = y \in \mathbb{R}^{N_L}$  at any  $x \in \mathbb{R}^{N_0}$  is determined through the following scheme:

$$\begin{aligned} h^{(0)} &:= x, \\ h^{(\ell)} &:= \rho(A_\ell h^{(\ell-1)} + b_\ell), \quad \forall \ell \in \{1, 2, \dots, L-1\}, \\ y &:= A_L h^{(L-1)} + b_L. \end{aligned} \quad (28)$$

The map

$$\mathcal{R} : \mathcal{S} \rightarrow C(\mathbb{R}^{N_0}, \mathbb{R}^{N_L}) \quad (29)$$

is called the realization map. Note that, with slight abuse of notation, the action of  $\rho$  on vectors in (28) is defined componentwise, i.e., for  $\ell \in \{1, 2, \dots, L-1\}$ ,

$$\rho(h) := (\rho(h_1), \rho(h_2), \dots, \rho(h_{N_\ell}))^T \in \mathbb{R}^{N_\ell}, \quad \forall h = (h_1, h_2, \dots, h_{N_\ell})^T \in \mathbb{R}^{N_\ell}.$$

Also, for the sake of notational simplicity, we have omitted the dependence of  $\mathcal{R}$  on the activation function  $\rho$ , since the latter is assumed fixed once it is chosen.

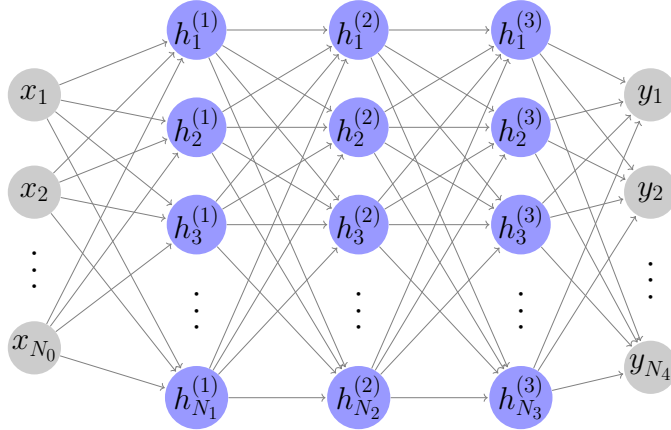


Figure 1: Illustration of neural networks with  $L = 4$  layers (i.e., three hidden layers).

### 3 Numerical algorithm

Based on the variational formulation (22)–(23), in this section we propose a numerical algorithm for solving the eigenpairs  $((\lambda_i, \varphi_i))_{1 \leq i \leq K}$  of the PDE problem (3) by training artificial neural networks introduced in Section 2.3. Before presenting the algorithm, let us first discuss the numerical treatment of both the constraints and the (high-dimensional) integrals in (22)–(23).

First, we consider the constraints involved in (22)–(23). Note that the minimization (22) is over functions with zero means (see the definition of  $\mathcal{H}^1$  in (14)) such that the pairwise orthonormality condition (23) holds. In practice, given  $f \in L^2(\mu)$ , the zero mean condition can be easily imposed by applying a shift operation to  $f$ , that is, by considering the function  $f - \mathbf{E}_\mu f$ . For functions  $f_1, f_2, \dots, f_K \in L^2(\mu)$ , we denote

$$f_i^{\text{center}} := f_i - \mathbf{E}_\mu f_i, \quad 1 \leq i \leq K. \quad (30)$$

Then, concerning the pairwise orthonormality condition (23), using the def-

inition (10) we find that the following two conditions are equivalent:

$$\text{cov}_\mu(f_i, f_j) = \delta_{ij}, \forall 1 \leq i, j \leq K \iff (f_i^{\text{center}})_{1 \leq i \leq K} \text{ satisfy (23)}. \quad (31)$$

In other words, once  $(f_i)_{1 \leq i \leq K}$  satisfy the condition on the left hand side of (31), the functions  $(f_i^{\text{center}})_{1 \leq i \leq K}$  satisfy both the zero mean condition and the pairwise orthonormality condition (23). As we will see below, this fact allows us to work with the unshifted functions  $(f_i)_{1 \leq i \leq K}$  when we train neural networks in the algorithm. The eigenfunctions with zero means can be easily recovered according to (30).

Next, we consider the approximation of the integrals in (22)–(23), or the mathematical expectation (8) in a general form. We discuss estimators based on a reweighting technique that is useful in alleviating sampling difficulties by allowing the use of biased sample data (see [2, 37] for similar techniques). Let  $\bar{\mu}$  be a probability measure in  $\mathbb{R}^d$  such that  $\mu$  (2) is absolutely continuous with respect to  $\bar{\mu}$ . By a change of measures, we have

$$\mathbf{E}_\mu(f) = \int_{\mathbb{R}^d} f(x) \mu(dx) = \int_{\mathbb{R}^d} f(x) \frac{d\mu}{d\bar{\mu}}(x) \bar{\mu}(dx) = \mathbf{E}_{\bar{\mu}}\left(f \frac{d\mu}{d\bar{\mu}}\right), \quad (32)$$

for a measurable test function  $f : \mathbb{R}^d \rightarrow \mathbb{R}$ , where  $\mathbf{E}_{\bar{\mu}}$  denotes the expectation with respect to  $\bar{\mu}$ . Assume that  $n$  states  $(x^{(\ell)})_{1 \leq \ell \leq n} \subset \mathbb{R}^d$  are sampled according to  $\bar{\mu}$ , where  $n \in \mathbb{N}$ . Then, based on (32), we can approximate the mean  $\mathbf{E}_\mu(f)$  by the importance sampling estimator

$$\mathbf{E}^{\text{data}}(f) := \frac{\sum_{\ell=1}^n f(x^{(\ell)}) v_\ell}{\sum_{\ell=1}^n v_\ell}, \quad \text{where } v_\ell = \frac{d\mu}{d\bar{\mu}}(x^{(\ell)}), \quad \forall \ell \in \{1, 2, \dots, n\}. \quad (33)$$

Typically, we choose  $\bar{\mu}$  such that comparing to  $\mu$  it is easier to sample states according to  $\bar{\mu}$  (e.g., less metastability in  $\bar{\mu}$ ). At the same time,  $\bar{\mu}$  should not be too different from  $\mu$ , so that the weights  $(v_\ell)_{1 \leq \ell \leq n}$  in (33) are neither too small nor too large. One can simply use  $\bar{\mu} = \mu$  (i.e.,  $v_\ell = 1.0$ ) when sampling directly from  $\mu$  is not a difficult task. For the computation of the weights in practice, we refer to the discussions in the numerical example in Section 4.1, in the setting where the states are sampled from  $\bar{\mu} = \mu$ , and to the detailed discussions in the numerical example in Section 4.2 (see (51)), in the setting where the states are sampled from a biased simulation.

In practice, a subset of the sample data  $(x^{(\ell)})_{1 \leq \ell \leq n}$  (i.e., mini-batch) is often used in training neural networks. Corresponding to this setting, let us consider a sequence of indices <sup>1</sup>

$$\mathcal{I} = (\ell_i)_{1 \leq i \leq B}, \quad \text{where } \ell_i \in \{1, 2, \dots, n\}, \quad (34)$$

<sup>1</sup>Precisely,  $\mathcal{I}$  is a multiset, since the repetition of indices is allowed and their ordering is unimportant.

for some  $B \in \mathbb{N}$  and  $1 \leq B \leq n$ . Given the sample data  $(x^{(\ell)})_{1 \leq \ell \leq n}$ , the sequence  $\mathcal{I}$  (34) defines a mini-batch of batch-size  $B$ :

$$\mathcal{B} := (x^{(\ell_1)}, x^{(\ell_2)}, \dots, x^{(\ell_B)}), \quad (35)$$

with which we can approximate the mean  $\mathbf{E}_\mu(f)$  by

$$\mathbf{E}^{\text{data}, \mathcal{I}}(f) := \frac{\sum_{i=1}^B f(x^{(\ell_i)}) v_{\ell_i}}{\sum_{i=1}^B v_{\ell_i}}. \quad (36)$$

In the following we apply (36) to approximating the integrals that will be involved in our algorithm. Recall that the Rayleigh quotient is defined as

$$\mathcal{Q}(f) := \frac{\mathcal{E}(f)}{\text{var}_\mu(f)}, \quad \text{for } f \in L^2(\mu), \quad (37)$$

where  $\mathcal{E}(\cdot)$  is the energy (15) and  $\text{var}_\mu(\cdot)$  is the variance in (10). Given the mini-batch (35), we can approximate the quantities in both (10) and (37) by

$$\begin{aligned} \text{cov}_\mu^{\text{data}, \mathcal{I}}(f, g) &:= \mathbf{E}^{\text{data}, \mathcal{I}}(fg) - \mathbf{E}^{\text{data}, \mathcal{I}}(f) \mathbf{E}^{\text{data}, \mathcal{I}}(g), \\ \text{var}_\mu^{\text{data}, \mathcal{I}}(f) &:= \mathbf{E}^{\text{data}, \mathcal{I}}(f^2) - (\mathbf{E}^{\text{data}, \mathcal{I}}(f))^2, \\ \mathcal{Q}^{\text{data}, \mathcal{I}}(f) &:= \frac{\frac{1}{\beta} \mathbf{E}^{\text{data}, \mathcal{I}}((a \nabla f) \cdot \nabla f)}{\text{var}_\mu^{\text{data}, \mathcal{I}}(f)}, \end{aligned} \quad (38)$$

respectively, for functions  $f, g : \mathbb{R}^d \rightarrow \mathbb{R}$ .

With the above preparations, we are ready to present the learning task for computing the first  $K$  eigenpairs of  $-\mathcal{L}$ .

### Learning task for the first $K$ eigenpairs $((\lambda_i, \varphi_i))_{1 \leq i \leq K}$ .

Let  $\mathcal{S}$  be the neural network space (27) with the neural network architecture  $\mathcal{N} = (N_0, N_1, \dots, N_L)$  in (26), where  $L, N_0, N_1, \dots, N_L \in \mathbb{N}$ . We assume that  $N_0 = d$  and  $N_L = 1$ , since we want to approximate eigenfunctions which are from  $\mathbb{R}^d$  to  $\mathbb{R}$ . Given a  $C^1$ -smooth activation function  $\rho : \mathbb{R} \rightarrow \mathbb{R}$ , recall that  $\mathcal{R} : \mathcal{S} \rightarrow C(\mathbb{R}^d, \mathbb{R})$  is the realization map defined in (28)–(29). Let  $\alpha > 0$  be a positive (penalty) constant and  $(\omega_i)_{1 \leq i \leq K}$  be a decreasing sequence of positive numbers, i.e.,  $\omega_1 > \dots > \omega_K > 0$  (see the second item of Remark 3).

We approximate the  $K$  eigenfunctions  $(\varphi_i)_{1 \leq i \leq K}$  by the realizations  $(\mathcal{R}(\Phi_i))_{1 \leq i \leq K}$  of  $K$  neural networks  $(\Phi_i)_{1 \leq i \leq K} \subset \mathcal{S}$ , which are trained using the loss function

$$\begin{aligned} \text{Loss}(\Phi_1, \dots, \Phi_K; \mathcal{I}) &:= \sum_{i=1}^K \omega_i \mathcal{Q}^{\text{data}, \mathcal{I}}(\mathcal{R}(\Phi_i)) \\ &\quad + \alpha \sum_{1 \leq i < j \leq K} \left( \text{cov}_\mu^{\text{data}, \mathcal{I}}(\mathcal{R}(\Phi_i), \mathcal{R}(\Phi_j)) - \delta_{ij} \right)^2, \end{aligned} \quad (39)$$

---

**Algorithm 1** Compute the first  $K$  eigenpairs  $((\lambda_i, \varphi_i))_{1 \leq i \leq K}$ .

---

- 1: **Data:**  $(x^{(\ell)})_{1 \leq \ell \leq n}$  and their weights  $(v_\ell)_{1 \leq \ell \leq n}$  (see (33)).
  - 2: **Parameters:** decreasing sequence  $(\omega_i)_{1 \leq i \leq K}$ , neural network space  $\mathcal{S}$ , total number of training steps  $J$ , penalty parameter  $\alpha$ , learning rate  $r$ , batch-size  $B$ .
  - 3: **Initialization:**  $\Phi_1^{(0)}, \Phi_2^{(0)}, \dots, \Phi_K^{(0)} \in \mathcal{S}$ . Set  $j = 0$ .
  - 4: **while**  $j < J$  **do**
  - 5:   Randomly generate the sequence  $\mathcal{I}^{(j)}$  of length  $B$  as in (34), and let  $\mathcal{B}^{(j)}$  be the corresponding mini-batch in (35).
  - 6:   Estimate the eigenpairs  $((\lambda_i^{(j)}, \varphi_i^{(j)}))_{1 \leq i \leq K}$  by (41).
  - 7:   (optional) Sort  $(\Phi_i^{(j)})_{1 \leq i \leq K}$  such that the eigenvalues  $\lambda_1^{(j)}, \dots, \lambda_K^{(j)}$  are non-decreasing.
  - 8:   Evaluate the loss (39) using the mini-batch  $\mathcal{B}^{(j)}$  by auto-differentiation.
  - 9:   Compute the gradient of the loss with respect to neural network parameters by auto-differentiation.
  - 10:   Update  $\Phi_1^{(j)}, \Phi_2^{(j)}, \dots, \Phi_K^{(j)}$  according to the gradient in Step 9 to get  $\Phi_1^{(j+1)}, \Phi_2^{(j+1)}, \dots, \Phi_K^{(j+1)}$ .
  - 11: **end while**
  - 12: **Output:** statistics based on the estimations recorded in Step 6.
- 

where  $\mathcal{I}$  is a sequence of indices generated randomly (see (34)),  $\mathcal{Q}^{\text{data}, \mathcal{I}}(\cdot)$  and  $\text{cov}_\mu^{\text{data}, \mathcal{I}}(\cdot, \cdot)$  are the quantities defined in (38) using the min-batch (35). In other words, we define the loss function (39) based on the variational formulation (22)–(23) in Theorem 1, where the constraints in (23) are imposed by adding quadratic penalty terms in (39) (see (31)). In particular, when  $K = 1$ , we obtain the learning task for the first eigenpair  $(\lambda_1, \varphi_1)$  with the loss

$$\text{Loss}(\Phi; \mathcal{I}) := \mathcal{Q}^{\text{data}, \mathcal{I}}(\mathcal{R}(\Phi)) + \alpha \left( \text{var}_\mu^{\text{data}, \mathcal{I}}(\mathcal{R}(\Phi)) - 1 \right)^2. \quad (40)$$

Denote by  $(\Phi_i^{(j)})_{1 \leq i \leq K}$  and  $\mathcal{I}^{(j)}$  the neural networks and the sequence of indices (34) in  $j$ th training step, respectively, where  $j \geq 0$ . The first  $K$  eigenpairs can be estimated by

$$\begin{aligned} \lambda_i^{(j)} &:= \mathcal{Q}^{\text{data}, \mathcal{I}^{(j)}}(\mathcal{R}(\Phi_i^{(j)})), \\ \varphi_i^{(j)} &:= \mathcal{R}(\Phi_i^{(j)}) - \mathbf{E}^{\text{data}, \mathcal{I}^{(j)}}(\mathcal{R}(\Phi_i^{(j)})), \end{aligned} \quad (41)$$

for  $i \in \{1, 2, \dots, K\}$ . The complete algorithm for training the neural networks is summarized in Algorithm 1.

We conclude this section with the following remarks.

**Remark 2.** *Two comments on the above training task are in order.*

1. Note that, instead of the Rayleigh quotient (37), one can also use the energy  $\mathcal{E}$  (15) in the loss function (39).
2. Because the Rayleigh quotient  $\mathcal{Q}(f)$  (37) (respectively, the energy  $\mathcal{E}(f)$  (15)) involves the spatial derivatives of the function  $f$ , the loss function (39) involves spatial derivatives of the realizations  $(\mathcal{R}(\Phi_i))_{1 \leq i \leq K}$  of neural networks. For this reason, we choose the activation function  $\rho$  to be  $C^1$ -smooth. Also, in Step 8 of Algorithm 1, we need to use auto-differentiation to compute the spatial derivatives of  $(\mathcal{R}(\Phi_i))_{1 \leq i \leq K}$  in order to evaluate the loss function.

**Remark 3.** We discuss the choices of the parameters  $K$ ,  $(\omega_i)_{1 \leq i \leq K}$  and  $\alpha$ .

1. Concerning the choice of  $K$ , Algorithm 1 works in principle for any  $K \in \mathbb{N}$ . In practice, however, one should choose  $K$  depending on the concrete problems under consideration and also taking the computational cost into account (the computational cost is larger for larger  $K$ ). For many metastable molecular systems, the eigenvalue problem has  $k$  small eigenvalues  $0 < \lambda_1 \leq \lambda_2 \leq \dots \leq \lambda_k$  for some  $k \in \mathbb{N}$  and there is a spectral gap between  $\lambda_k$  and  $\lambda_{k+1}$ . For these applications, it is appropriate to apply Algorithm 1 with some  $K \in \{1, \dots, k\}$ .
2. Although Theorem 1 holds for non-increasing sequences  $\omega_1 \geq \omega_2 \geq \dots \geq \omega_K > 0$ , in practice, choosing  $(\omega_i)_{1 \leq i \leq K}$  to be pairwise distinct, i.e.,  $\omega_1 > \omega_2 > \dots > \omega_K > 0$ , can help avoid the non-uniqueness of the minimizer due to reordering of eigenfunctions. For problems where the true eigenvalues  $\lambda_1, \dots, \lambda_K$  are of the same order, Algorithm 1 works well for different sequences  $(\omega_i)_{1 \leq i \leq K}$  as long as the ratio  $\frac{\omega_K}{\omega_1}$  is not too small (so that each eigenvalue has similar contribution to the total loss in (38)). Even when the true eigenvalues have different orders of magnitude, Algorithm 1 works by choosing the parameters  $(\omega_i)_{1 \leq i \leq K}$  properly (see the alanine dipeptide example in Section 4.2).
3. A large  $\alpha$  is required in Algorithm 1 in order to guarantee that the constraints are imposed effectively. However, a too large  $\alpha$  would introduce stiffness which in turn restricts the size of the learning rate in training. As an example, when the coefficients  $(\omega_i)_{1 \leq i \leq K}$  are chosen such that  $\sum_{i=1}^K \omega_i \lambda_i$  are below 5 (as  $(\lambda_i)_{1 \leq i \leq K}$  are unknown, this may require some empirical estimates in practice), then  $\alpha \in [20, 50]$  would be an appropriate choice.

## 4 Numerical examples

In this section, we study two concrete examples in order to demonstrate Algorithm 1. The code used to produce the numerical results in this section is available at <https://github.com/zwpku/EigenPDE-NN>.

## 4.1 A high-dimensional model problem

In the first example, we consider an eigenvalues problem whose leading eigenvalues can be computed using traditional numerical methods. This example allows us to compare the solutions given by Algorithm 1 to the solutions computed by traditional numerical methods (i.e., reference solutions). We consider the problem (3) for different dimensions  $d = 2, 50, 100$ . In each case, we chose  $\beta = 1.0$  and we fix the matrix  $a$  in (4) as the identity matrix. Correspondingly, the generator (4) is

$$\mathcal{L}_d f = -\nabla V_d \cdot \nabla f + \Delta f \quad (42)$$

for a test function  $f : \mathbb{R}^d \rightarrow \mathbb{R}$ , where  $V_d : \mathbb{R}^d \rightarrow \mathbb{R}$  for  $d = 2, 50, 100$  are the potential functions that we explain next.

**Potentials  $V_d$  for  $d = 2, 50, 100$ .** First, let us consider the case where  $d = 2$ . The potential  $V_2 : \mathbb{R}^2 \rightarrow \mathbb{R}$  is defined as

$$V_2(x_1, x_2) = V(\theta) + 2(r - 1)^2 + 5e^{-5r^2}, \quad \forall (x_1, x_2) \in \mathbb{R}^2, \quad (43)$$

where  $(\theta, r) \in [-\pi, \pi) \times [0, +\infty)$  are the polar coordinates which are related to  $(x_1, x_2) \in \mathbb{R}^2$  by

$$x_1 = r \cos \theta, \quad x_2 = r \sin \theta, \quad (44)$$

and  $V : [-\pi, \pi) \rightarrow \mathbb{R}$  is a double-well potential function defined as

$$V(\theta) = \begin{cases} [1 - (\frac{3\theta}{\pi} + 1)^2]^2, & \theta \in [-\pi, -\frac{\pi}{3}), \\ \frac{1}{5}(3 - 2 \cos(3\theta)), & \theta \in [-\frac{\pi}{3}, \frac{\pi}{3}), \\ [1 - (\frac{3\theta}{\pi} - 1)^2]^2, & \theta \in [\frac{\pi}{3}, \pi). \end{cases} \quad (45)$$

As shown in the right plot of Figure 2, there are three low-energy regions on the potential surface of  $V_2$ , which are labelled as  $A$ ,  $B$ , and  $C$ . Each of the two regions  $A$  and  $B$  contains a global minimum point of  $V_2$  (i.e., both of these two minimum points attain the same lowest potential value), while the region  $C$  contains a local minimum point of  $V_2$ .

Next, for  $d = 50$  and  $d = 100$ , we define  $V_d : \mathbb{R}^d \rightarrow \mathbb{R}$  as the sum of  $V_2$  in the first two coordinates of the state and a Gaussian potential in the other coordinates, namely,

$$V_d(x) = V_2(x_1, x_2) + 5 \sum_{i=3}^d x_i^2, \quad \forall x = (x_1, x_2, \dots, x_d) \in \mathbb{R}^d. \quad (46)$$

Roughly speaking, the coefficient 5 in front of the Gaussian term in (46) is introduced such that the dynamics of the coordinates  $(x_3, \dots, x_d)$  under the potential  $V_d$  reaches quasi-equilibrium in a sufficiently short time. This in turn guarantees that the three smallest eigenvalues  $\lambda_1$ ,  $\lambda_2$ , and  $\lambda_3$  of  $-\mathcal{L}_d$ ,

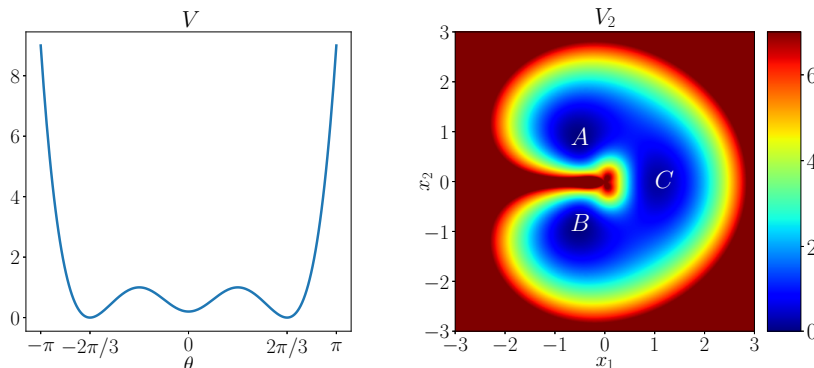


Figure 2: Profiles of the potential  $V$  (45) (left) and the two-dimensional potential  $V_2$  (43) (right) in the first example. There are three low-energy regions on the potential surface of  $V_2$ , which are labelled as  $A$ ,  $B$ , and  $C$ . Regions  $A$  and  $B$  contain global minimum points of  $V_2$ , whereas the region  $C$  contains a local minimum point of  $V_2$ .

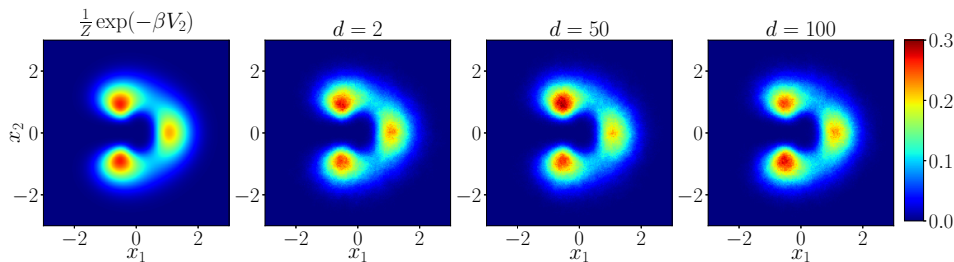


Figure 3: Empirical densities in the first example. First plot: the probability density  $\frac{1}{Z}e^{-\beta V_2}$ , where  $\beta = 1$  and  $V_2$  is the potential function defined in (43) (see its profile in Figure 2). Second plot: empirical probability density of the sample data for  $d = 2$ . Third and fourth plots: empirical marginal probability densities of the sample data in the first two coordinates  $(x_1, x_2)$  for  $d = 50$  and  $d = 100$ , respectively. In each of the last three plots,  $n = 5 \times 10^6$  states are sampled using the Euler-Maruyama scheme with the timestep  $\Delta t = 0.001$ .

where  $d = 50, 100$ , are the same as those when  $d = 2$ , so that we can use the solution given by the finite volume method for  $d = 2$  (see (47) below) as the reference solution to the eigenvalue PDE (3) for dimensions  $d = 50, 100$  as well. Correspondingly, for both  $d = 50$  and  $d = 100$ , the first three eigenfunctions  $\varphi_1, \varphi_2, \varphi_3$  are functions of the first two coordinates  $(x_1, x_2)$  only, and can be compared to the eigenfunctions obtained using the finite volume method for  $d = 2$ .



	FVM, $d = 2$	NN, $d = 2$	NN, $d = 50$	NN, $d = 100$
$\lambda_1$	0.219	0.226 (0.003)	0.210 (0.002)	0.220 (0.003)
$\lambda_2$	0.764	0.768 (0.006)	0.751 (0.007)	0.749 (0.006)
$\lambda_3$	2.790	2.810 (0.017)	2.725 (0.022)	2.737 (0.020)

Table 1: Estimations of the eigenvalues  $\lambda_1, \lambda_2, \lambda_3$  in the first example. Column “FVM,  $d = 2$ ” shows the numerical solutions obtained using the finite volume method for  $d = 2$  (see (47)). Columns with labels “NN,  $d = 2$ ”, “NN,  $d = 50$ ”, and “NN,  $d = 100$ ” show the means and the sample standard deviations (in brackets) of the eigenvalues estimated in the last 100 training steps of Algorithm 1 for  $d = 2$ ,  $d = 50$ , and  $d = 100$ , respectively. The potential function is  $V_2$  (43) for  $d = 2$ , whereas the potential functions  $V_d$  for  $d = 50$  and  $d = 100$  are defined in (46).

**Reference solution for  $d = 2$ .** Since (3) is a two-dimensional eigenvalue PDE problem when  $d = 2$ , the eigenvalues of  $-\mathcal{L}_2$ , given by (42), can be solved numerically using the finite volume method [32]. Specifically, taking into account the profile of the potential surface of  $V_2$  (see the right plot of Figure 2), we truncate the space  $\mathbb{R}^2$  to the finite domain  $[-3.0, 3.0] \times [-3.0, 3.0]$ , on which the PDE (3) is discretized using a grid of size  $400 \times 400$  (see [72] for details of the discretization). The discretized matrix eigenvalue problem is then solved using Krylovschur method implemented in `slepc4py`, which is a Python binding for the package SLEPc [22]. In this way, we obtain the first three eigenvalues as

$$\lambda_1 = 0.219, \quad \lambda_2 = 0.764, \quad \lambda_3 = 2.790. \quad (47)$$

These values in (47) remain unchanged when we enlarge the truncated domain and when we refine the grid used for discretization. The corresponding eigenfunctions  $\varphi_1, \varphi_2, \varphi_3$  obtained using the finite volume method are shown in the first column of Figure 4.

**Solutions for  $d = 2, 50$ , and 100 using neural networks.** Next, we use Algorithms 1 to compute the first three eigenpairs of  $-\mathcal{L}_d$  (42) for dimensions  $d = 2, d = 50$  and  $d = 100$ , respectively.

For each  $d \in \{2, 50, 100\}$ , the invariant measure  $\mu$  corresponding to the generator  $\mathcal{L}_d$  has the density  $\frac{1}{Z}e^{-\beta V_d}$ , where  $Z$  is the normalizing constant (depending on  $d$ ). We first generate  $n = 5 \times 10^6$  states in  $\mathbb{R}^d$  from the scheme

$$x^{(\ell)} = x^{(\ell-1)} - \nabla V_d(x^{(\ell-1)}) \Delta t + \sqrt{2\beta^{-1}\Delta t} \boldsymbol{\eta}^{(\ell)}, \quad \ell = 1, 2, \dots, n, \quad (48)$$

starting from some initial state  $x^{(0)} \in \mathbb{R}^d$ , where the timestep  $\Delta t = 0.001$  and  $\boldsymbol{\eta}^{(\ell)} \in \mathbb{R}^d$ ,  $1 \leq \ell \leq n$ , are i.i.d. standard Gaussian variables in  $\mathbb{R}^d$ . Note that (48) is just the Euler-Maruyama scheme of the SDE (1) when both  $a$

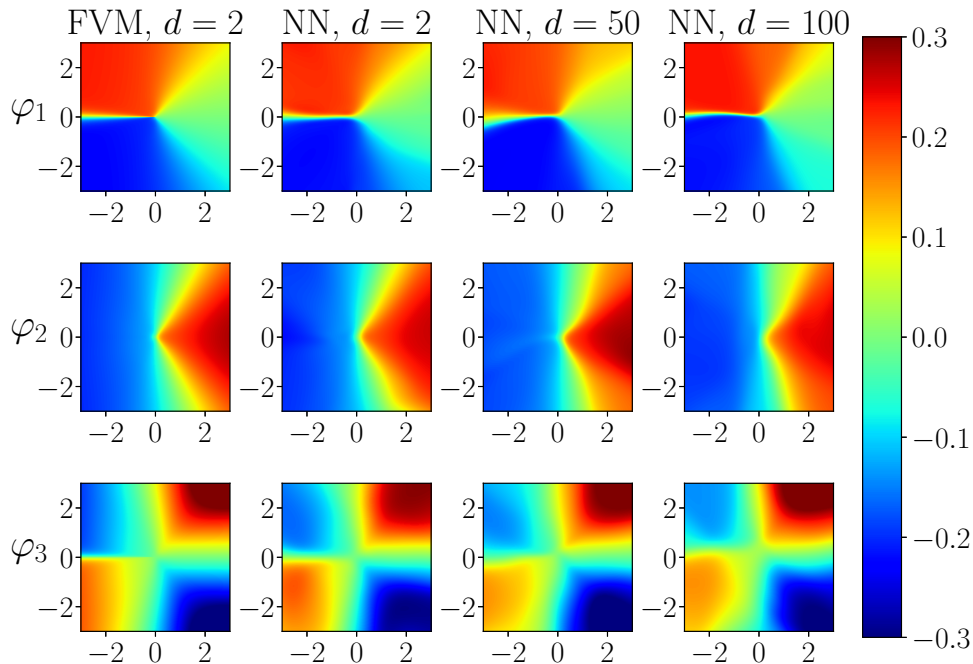


Figure 4: The first three eigenfunctions  $\varphi_1, \varphi_2, \varphi_3$  in the first example, computed using the finite volume method for  $d = 2$  (column “FVM,  $d = 2$ ”) and by training neural networks using Algorithm 1 for  $d = 2$  (column “NN,  $d = 2$ ”),  $d = 50$  (column “NN,  $d = 50$ ”), and  $d = 100$  (column “NN,  $d = 100$ ”), respectively. The last three columns show the trained eigenfunctions after  $J = 7100$  training steps using Algorithm 1. For  $d = 50$  and  $d = 100$ , the third and the fourth columns show the eigenfunctions  $\varphi_1, \varphi_2, \varphi_3$  as functions in the first two coordinates  $x_1, x_2$ , where the remaining coordinates  $(x_3, \dots, x_d)$  are randomly selected according to certain centered Gaussian distribution.

and  $\sigma$  are the identify matrix. In this example we do not use the reweighting technique introduced in Section 3, since it is not difficult to sample states directly from the numerical scheme (48) whose invariant measure approximates  $\mu$ . In other words, we have  $v_\ell = 1$  for  $1 \leq \ell \leq n$ , where  $v_\ell$  are the weights in (33). As shown in Figure 3, the empirical (marginal) probability densities of the sampled trajectory data in  $(x_1, x_2)$  are accordant with the probability density  $\frac{1}{Z}e^{-\beta V_2}$ . This implies that the trajectories are sufficiently long, so that the empirical estimator (33), as well as the estimator (36) for large batch-sizes, are good approximations of the true mean value  $\mathbf{E}_\mu(f)$  (for reasonable functions  $f$ ).

Using the sampled states as training data, we apply Algorithm 1 to estimate the first three eigenpairs. We set  $K = 3$ , the penalty parameter

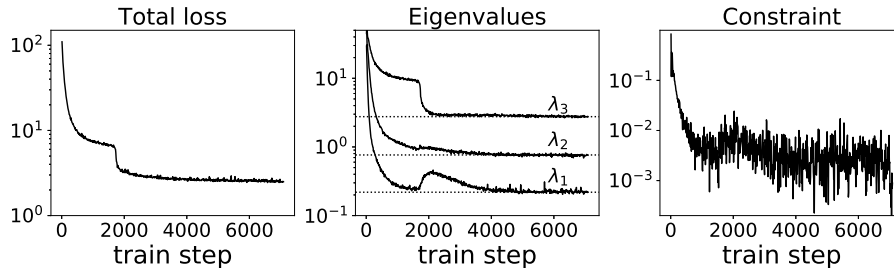


Figure 5: The evolution of quantities during the training procedure in the first example, where  $d = 100$ . Left: the loss function (39). Middle: estimations of the eigenvalues  $\lambda_1$ ,  $\lambda_2$ , and  $\lambda_3$ . The dotted horizontal lines show the reference solutions (47) obtained using the finite volume method. Right: the quantity  $\mathcal{C}$  in (50) which corresponds to the penalty term in (39).

$\alpha = 20$ , and the coefficients  $\omega_1 = 1.0$ ,  $\omega_2 = 0.8$ , and  $\omega_3 = 0.6$  in the loss function (39). For each  $d \in \{2, 50, 100\}$ , each of the first three eigenfunctions is represented by a neural network with the same network architecture

$$\mathcal{N} = (d, 20, 20, 20, 1). \quad (49)$$

In other words, the neural network has one input layer of size  $d$ , three hidden layers of size 20, and one output layer of size 1 (see Figure 1 for the illustration of neural networks). We use the activation function  $\rho(x) = \tanh x$ . In each test, in order to train the neural network,  $J = 7100$  training steps are performed using the Adam optimization method [26] with learning rate  $r = 0.005$ . The batch-size  $B = 5000$  is used for the first 7000 steps. The eigenvalues are computed (see Table 1) as the mean values of the estimations in the final 100 training steps, i.e., from step 7001 to step 7100, where a large batch-size  $B = 20000$  is adopted. As seen from Table 1 and Figure 4, Algorithm 1 is able to approximate the first three eigenvalues in (47) and their corresponding eigenfunctions. For  $d = 50, 100$ , by inspecting the eigenfunctions at coordinates  $(x_3, \dots, x_d)$  that are randomly sampled according to certain centered Gaussian distribution, we find that they depend on the values of  $(x_3, \dots, x_d)$  rather weakly (see the last two columns of Figure 4). Although the potentials (46) in this example are relatively simple, it is interesting to note that, by training neural networks with fully connected architecture (49), Algorithms 1 is able to identify the eigenfunctions which are functions of  $(x_1, x_2)$  only. Figure 5 shows the evolution of the loss function (39), the estimations of eigenvalues using (41) (see Step 6 of Algorithm 1), and the quantity

$$\mathcal{C} = \sum_{1 \leq i \leq j \leq K} \left( \text{cov}_\mu^{\text{data}, \mathcal{I}} (\mathcal{R}(\Phi_i), \mathcal{R}(\Phi_j)) - \delta_{ij} \right)^2 \quad (50)$$

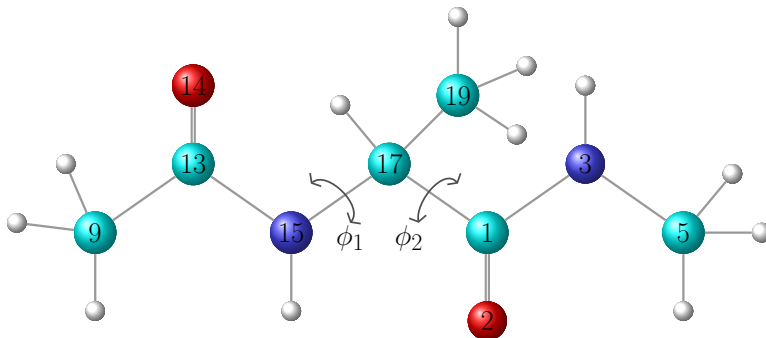


Figure 6: Alanine dipeptide in vacuum. The 22 atoms of the system as well as the two dihedral angles  $\phi_1, \phi_2$  are shown. The hydrogen atoms, carbon atoms, nitrogen atoms and oxygen atoms are displayed in gray, cyan, blue, and red, respectively. The indices of the 10 non-hydrogen atoms are given by the numbers.

during the training procedure in the case where  $d = 100$ . The results for  $d = 2, 50$  are similar and therefore they are not shown here. The quantity  $\mathcal{C}$  in (50) corresponds to the penalty term in the loss function (39). One can observe from Figure 5 that both the loss function and the eigenvalues converge within 5000 training steps. The quantity  $\mathcal{C}$  (50) is fluctuating during the training procedure due to the use of both mini-batch and the finite penalty parameter  $\alpha = 20$ . Nevertheless, the magnitude of  $\mathcal{C}$  stays below  $10^{-2}$  in most of the training steps, indicating that the constraints are well imposed during the training procedure. Finally, we note that very similar results were obtained when we carried out the same numerical experiment with a larger network architecture  $\mathcal{N} = (d, 25, 25, 25, 25, 1)$ .

## 4.2 Alanine dipeptide

In the second example, we study the simple molecular system alanine dipeptide in vacuum. The system consists of 22 atoms. Since each atom has three coordinates, the full state of the system has dimension 66. It is known that the dynamics of the system can be well described using two dihedral angles  $\phi_1, \phi_2$  (see Figure 6). The system exhibits three metastable conformations, which are often named as C5, C7eq and C7ax (see Figure 7). The transition between the two conformations C7eq and C7ax occurs much more rarely comparing to the transition between the conformations C5 and C7eq.

We generate the trajectory data of the system using the NAMD software package [54]. In all the simulations below, the system is simulated using Langevin dynamics at the temperature  $T = 300$  K with the damping coefficient  $1 \text{ s}^{-1}$  and the timestep 1 fs. The dynamics of the system in

the position space is ergodic with respect to the unique invariant distribution  $\mu$  (2) for some potential function  $V : \mathbb{R}^{66} \rightarrow \mathbb{R}$ , where  $\beta = (k_B T)^{-1} = 1.678(\text{kcal/mol})^{-1}$  and  $k_B$  denotes the Boltzmann constant. The initial state of the system is prepared by performing 500 energy minimization steps followed by  $10^6$  equilibration steps (i.e., 1 ns). Due to the metastability of the system, unbiased molecular dynamics simulation is computationally expensive for generating trajectory data that is distributed according to the invariant distribution  $\mu$ . Therefore, we use the reweighting technique discussed in Section 3 and we sample the data from a biased simulation. Specifically, the training data and the test data are prepared in the following three steps.

- (1) *Computation of mean force and its potential using ABF.* In the first step, we simulate the system for 20 ns using the adaptive biasing force (ABF) method [11, 20, 10] that is implemented in the **colvar** module of the NAMD package [15]. The two dihedral angles  $\phi_1, \phi_2$  are used as collective variables in the ABF method, whose space  $[-180^\circ, 180^\circ) \times [-180^\circ, 180^\circ)$  is discretized with grid size  $5^\circ$ . During the simulation, the mean force in each cell of the discretized grid of the dihedral angles is estimated using samples that fall in the cell, and is applied to the system (when the system visits the cell) after 100 samples are collected. After the simulation, we obtain the mean force and its potential  $V_{\text{PMF}}$ , i.e., the potential of mean force (PMF), on the discrete grid of the dihedral angles (see Figure 7).
- (2) *Biasing force by rescaling the mean force.* As one can see in Figure 7, the magnitude of the potential  $V_{\text{PMF}}$  is quite large. In this step, we rescale the mean force obtained in the previous step by  $\eta = 0.7$ . Accordingly, the potential of the rescaled mean force is  $V_{\text{bias}} = 0.7V_{\text{PMF}}$ .
- (3) *Training data and test data by molecular dynamics simulations under fixed biasing force.* We simulate the system for 100 ns using ABF, where the rescaled mean force in the previous step is applied to the system and is kept fixed during the simulation. The trajectory is recorded every 1 ps, resulting in a training data set  $(x^{(\ell)})_{1 \leq \ell \leq n}$  that consists of  $n = 10^5$  states. We denote by  $\phi_1^{(\ell)}, \phi_2^{(\ell)}$  the two dihedral angles  $\phi_1, \phi_2$  of the state  $x^{(\ell)} \in \mathbb{R}^{66}$  for  $\ell = 1, 2, \dots, n$ . Then, the weights

$$v_\ell = \frac{\exp(-\beta V_{\text{bias}}(\phi_1^{(\ell)}, \phi_2^{(\ell)}))}{\frac{1}{n} \sum_{\ell'=1}^n \exp(-\beta V_{\text{bias}}(\phi_1^{(\ell')}, \phi_2^{(\ell')}))}, \quad \ell \in \{1, 2, \dots, n\} \quad (51)$$

are used in estimating the mean values according to (33). See Figure 8 for the histogram of the angles  $(\phi_1^{(\ell)}, \phi_2^{(\ell)})_{1 \leq \ell \leq n}$  of the trajectory data and the profile of the weights as a function of the dihedral angles. Finally, we obtain the test data set of the same size by running another biased simulation independently with the same parameters.

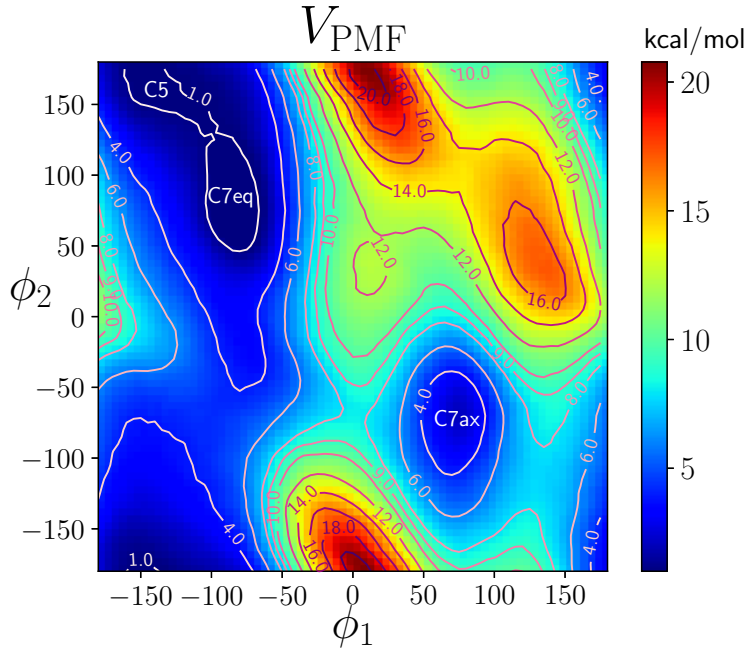


Figure 7: Potential of mean force  $V_{\text{PMF}}$  as a function of the two dihedral angles  $\phi_1, \phi_2$  of alanine dipeptide, computed using the adaptive biasing method in the NAMD package. The system has three metastable conformations, which are termed as C5, C7eq and C7ex, respectively. These three conformations correspond to the three regions where the value of the potential  $V_{\text{PMF}}$  is low.

Let us point out that, alternative to the ABF method, sampling techniques such as Metadynamics [30, 31], the extended system ABF (eABF) method [36] can be used in preparing data as well. It is also possible to employ sampling methods that do not require the knowledge of collective variables, such as the simulated tempering [41] and the replica exchange molecular dynamics [59]. However, in this case, the estimator (33) has to be modified in order to estimate the mean values in the loss function.

With the training data prepared above, we compute the leading eigenpairs of the problem (3) by applying Algorithm 1, where the generator is

$$\mathcal{L}f = -\frac{D}{k_B T} \nabla V \cdot \nabla f + D \Delta f \quad (52)$$

for a test function  $f : \mathbb{R}^{66} \rightarrow \mathbb{R}$ , and  $D > 0$  is the diffusion coefficient. Equivalently, we are considering the SDE

$$dx(s) = -\frac{D}{k_B T} \nabla V(x(s)) ds + \sqrt{2D} dw(s), \quad s \geq 0, \quad (53)$$

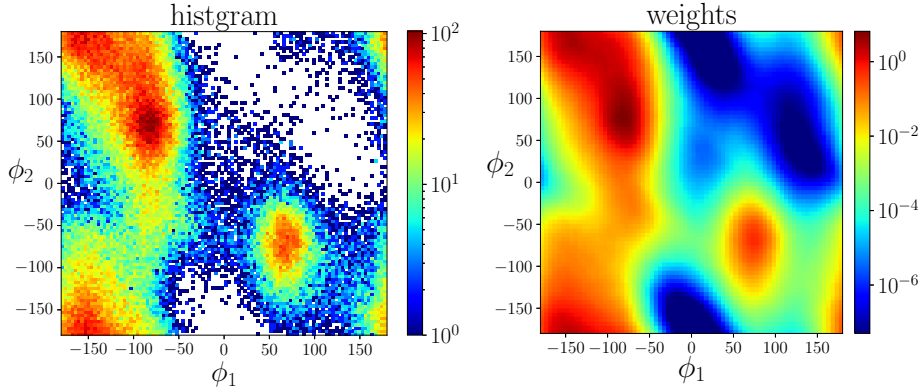


Figure 8: Left: histogram of the two dihedral angles  $\phi_1$  and  $\phi_2$  of alanine dipeptide. The system is simulated for 100 ns, under the fixed biasing force whose corresponding potential is  $V_{\text{bias}} = 0.7V_{\text{PMF}}$  (see Figure 7 for the profile of  $V_{\text{PMF}}$ ). By recording the states every 1 ps,  $10^5$  states of the trajectory are obtained in total, which are used to plot the histogram. Right: weights proportional to  $\exp(-\beta V_{\text{bias}})$  as a function of the dihedral angles (see (51)).

where  $x(s) \in \mathbb{R}^{66}$  and  $(w(s))_{s \geq 0}$  is a standard Brownian motion in  $\mathbb{R}^{66}$ . Without loss of generality, we assume that the indices of the coordinates  $x = (x_1, x_2, \dots, x_{66})$  are ordered in a way such that the coordinates of the non-hydrogen atoms are  $((x_{3(i-1)+1}, x_{3(i-1)+2}, x_{3(i-1)+3}))_{1 \leq i \leq 10}$ . We define  $\mathbf{x}_i = (x_{3(i-1)+1}, x_{3(i-1)+2}, x_{3(i-1)+3})$  for  $i \in \{1, 2, \dots, 10\}$  and set  $\mathbf{x} = (x_1, x_2, \dots, x_{10})^T$  (note that the ordering here is different from the indices in Figure 6). In the following numerical tests we choose  $D = 10^{-5} \text{ cm}^2/\text{s}$ .

As in the work [37, 2], we approximate the eigenfunctions by functions of  $\mathbf{x} \in \mathbb{R}^{30}$ , i.e., the coordinates of the 10 non-hydrogen atoms (see Figure 6). To guarantee the eigenfunctions after training are invariant under both rotations and translations, the Cartesian coordinates  $\mathbf{x}$  of the non-hydrogen atoms in the trajectory data are aligned with respect to the coordinates of the same predetermined reference configuration (such that the root mean squared deviation is minimized) before they are passed to the neural networks. Specifically, we define the map  $F_{\text{opt}} : \mathbb{R}^{30} \rightarrow \mathbb{R}^{30}$  as

$$F_{\text{opt}}(\mathbf{x}) = \left( (\mathbf{x}_1 - \mathbf{b}_{\text{opt}}(\mathbf{x}))A_{\text{opt}}(\mathbf{x}), (\mathbf{x}_2 - \mathbf{b}_{\text{opt}}(\mathbf{x}))A_{\text{opt}}(\mathbf{x}), \dots, (\mathbf{x}_{10} - \mathbf{b}_{\text{opt}}(\mathbf{x}))A_{\text{opt}}(\mathbf{x}) \right)^T, \quad (54)$$

where, for given  $\mathbf{x}$ ,  $A_{\text{opt}}(\mathbf{x}) \in \mathbb{R}^{3 \times 3}$ ,  $\mathbf{b}_{\text{opt}}(\mathbf{x}) \in \mathbb{R}^3$  are the optimal rotation matrix and the optimal translation vector, respectively, which minimize the root mean squared deviation of  $\mathbf{x}$  from the reference configuration. In practice,  $\mathbf{b}_{\text{opt}}(\mathbf{x})$  is easily determined by matching the centers of atoms, whereas

$A_{\text{opt}}(\mathbf{x})$  can be numerically computed using the Kabsch algorithm [25].

The eigenfunctions are approximated by functions that are of the form  $\mathcal{R}(\Phi) \circ F_{\text{opt}}(\mathbf{x})$ , where  $\Phi$  is a neural network with the network architecture

$$\mathcal{N} = (30, 20, 20, 20, 1). \quad (55)$$

In other words, the Cartesian coordinates  $\mathbf{x} \in \mathbb{R}^{30}$  of the non-hydrogen atoms are aligned using the map  $F_{\text{opt}}$  (54). Then, they are passed to the neural network which has three hidden layers of equal size 20 and one output layer of size 1. It is clear that the functions represented in the form above are invariant under both rotations and translations. As in the previous example, we use  $\rho(x) = \tanh x$  as the activation function.

We start by computing the first eigenpair  $(\lambda_1, \varphi_1)$  of  $-\mathcal{L}$  given in (52). We apply Algorithm 1 with  $K = 1$ , where we train the neural network using the Adam optimization method for  $J = 20000$  training steps. In all these 20000 steps, we use the batch-size  $B = 10000$ , the learning rate  $r = 0.001$ , and the penalty constant  $\alpha = 20$ . The mean of the first eigenvalue estimated in the last 4000 training steps is

$$\lambda_1 = 0.047 \text{ ns}^{-1}, \quad (56)$$

with the sample standard deviation  $0.005 \text{ ns}^{-1}$ . The eigenfunction  $\varphi_1$  approximated by the trained neural network at the end of the training procedure is shown in Figure 9. Specifically, in the left (right) plot in Figure 9, representative states in the training (test) data are placed in the angle space according to their dihedral angles  $\phi_1, \phi_2$  and are colored according to the values of the first eigenfunction  $\varphi_1$ . One clearly observes that the first eigenfunction  $\varphi_1$  given by Algorithm 1 is close to a constant within each of the metastable regions (see Figure 7). The profile of  $\varphi_1$  separates the conformation C7ax from the other two conformations C5 and C7eq. Moreover, comparing the two plots in Figure 9, we see that the eigenfunction  $\varphi_1$  has very similar profiles on both the training data and the test data, implying that the trained neural network (therefore the eigenfunction) has satisfactory generalizability. To further verify the numerical estimation of the eigenvalue  $\lambda_1$  in (56), we have repeated the numerical study with a different set of training data, sampled under the mean force that is rescaled by  $\eta = 0.8$  (correspondingly,  $V_{\text{bias}} = 0.8V_{\text{PMF}}$ ). In this case, the mean of  $\lambda_1$  estimated in the last 4000 training steps is  $\lambda_1 = 0.044 \text{ ns}^{-1}$ , with the sample standard deviation  $0.004 \text{ ns}^{-1}$ . Moreover, a numerical study was carried out using a larger network architecture  $\mathcal{N} = (30, 25, 25, 25, 25, 1)$ , which yields the mean value  $\lambda_1 = 0.045 \text{ ns}^{-1}$ , with the sample standard deviation  $0.006 \text{ ns}^{-1}$ . These numerical experiments confirm that the numerical estimation in (56) is stable with different choices of training data and neural network architectures.

We have also computed the second eigenpair  $(\lambda_2, \varphi_2)$  by applying Algorithm 1 with  $K = 2$ . Knowing a priori that the magnitude of the second



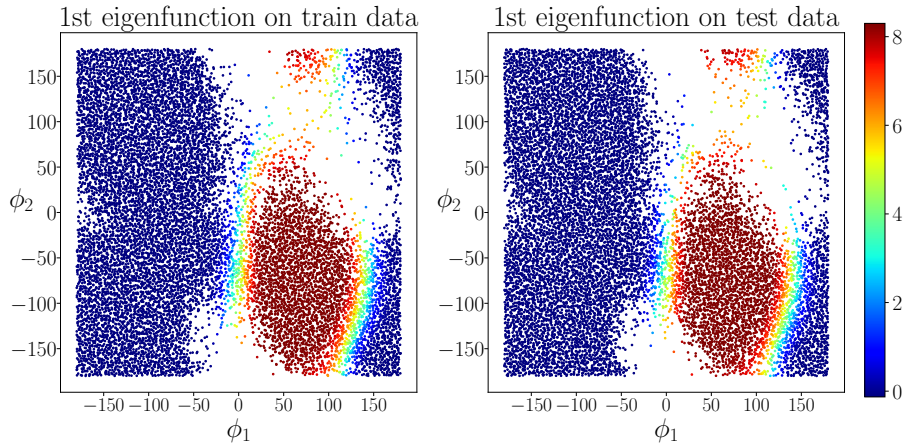


Figure 9: For the alanine dipeptide example, the first eigenfunction  $\varphi_1$  learned by training the neural network using Algorithm 1 is evaluated on the training data (left) and on the test data (right). Selected states in the data sets are positioned as points according to their dihedral angles  $\phi_1, \phi_2$ , and are colored according to the values of the first eigenfunction  $\varphi_1$ .

eigenvalue  $\lambda_2$  (which corresponds to the transition between C5 and C7eq; see the discussion below) is much larger than that of  $\lambda_1$  in (56), in this test we choose the coefficients  $\omega_1 = 1.0$  and  $\omega_2 = 0.05$ . All the other parameters are the same as those used in the previous test for computing the first eigenpair. After training the neural networks, we obtain numerical results of the first two eigenpairs. For the first eigenpair, both the estimation of  $\lambda_1$  and the profile of the eigenfunction  $\varphi_1$  are very close to the results obtained in the previous test. See (56) and Figure 9, respectively. For the second eigenpair, the mean of the eigenvalue  $\lambda_2$  estimated in the last 4000 training steps is

$$\lambda_2 = 23.92 \text{ ns}^{-1}, \quad (57)$$

with the sample standard deviation  $0.60 \text{ ns}^{-1}$ . Similar as in the previous test, the left (right) plot of Figure 10 shows the second eigenfunction  $\varphi_2$  at representative states in the training (test) data set. In contrast to the first eigenfunction  $\varphi_1$  (Figure 9), the values of the second eigenfunction  $\varphi_2$  have different signs in the two conformational regions corresponding to C5 and C7eq (see Figure 7 and recall the periodic boundary conditions). This indeed confirms that the second eigenpair is linked to the transitional events of alanine dipeptide between the two conformations C5 and C7eq. The fact that the estimated second eigenvalue  $\lambda_2$  in (57) is much larger than  $\lambda_1$  in (56) is also consistent with the fact that the transition between C5 and C7eq is much more frequent than the transition to C7ax.

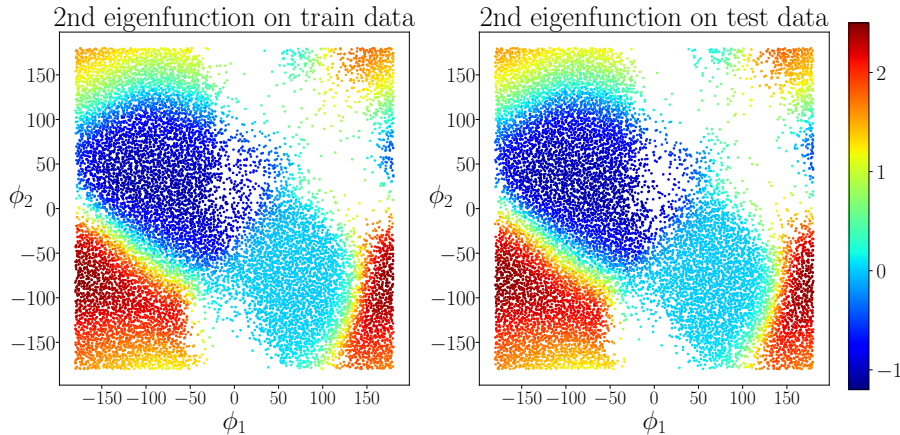


Figure 10: For the alanine dipeptide example, the second eigenfunction  $\varphi_2$  learned by training neural networks using Algorithm 1 is evaluated on the training data (left) and on the test data (right). Selected states in the data sets are positioned as points according to their dihedral angles  $\phi_1, \phi_2$ , and are colored according to the values of the second eigenfunction  $\varphi_2$ .

## 5 Conclusion and Discussions

In this paper, we have studied numerical methods for solving high-dimensional eigenvalue PDEs by training artificial neural networks. The algorithm proposed in this work allows us to compute multiple eigenvalues and the corresponding eigenfunctions of the eigenvalue PDEs. The numerical experiments on two concrete examples demonstrate the capability of the method in estimating large timescales and unveiling the transition mechanism of high-dimensional metastable diffusion processes. In the following we discuss several related research topics that we would like to consider in future work.

*Learning collective variables for complex molecular systems.* Various approaches have been developed in recent years for finding good collective variables of molecular systems [40, 16, 8, 6, 2]. Related to the current work, the previous work [71] argued that the leading eigenfunctions of the system’s generator provide collective variables that are optimal in certain sense. In future work, we will apply the algorithm developed in the current work in devising novel numerical approaches for the discovery of the collective variables of molecular systems.

*Application to eigenvalue problems in quantum physics.* Schrödinger eigenvalue problems play a central role in quantum physics. Thanks to the powerful capability of neural networks, numerical algorithms for solving high-dimensional Schrödinger eigenvalue problems are gaining research attentions in recent years [39, 19, 21, 53, 46, 24]. Also see [29] for an earlier

work. In future, we will consider applying our numerical algorithm in solving quantum eigenvalue problems. In particular, its potential application in computing the excited states of quantum systems will be explored.

*Alternative methods for training under constraints.* In our algorithm, the constraints on the eigenfunctions are imposed softly using penalty method. This leads to a simple unconstrained training task, which however involves a penalty constant  $\alpha$  that has to be determined empirically. Although we find that our algorithm performs well in practice for a wide range of  $\alpha$ , it is expected that the choice of  $\alpha$  indeed plays a role in the training procedure. Very large  $\alpha$  would introduce stiffness to the problem which in turn restricts the size of the learning rate in training, whereas a very small  $\alpha$  would make the constraints ineffective. In future work, we will study the dependence of the algorithm on  $\alpha$ , as well as alternative methods for handling constraints, such as sampling schemes with constraints [70, 35], the conditional gradient method and its variants [56, 1], and the constrained training algorithms for neural networks [33].

*Application to more sophisticate molecular dynamics applications.* In this work we have tested our algorithm on simple alanine dipeptide molecular system. Based on these experience, more sophisticate molecular systems will be studied in the next step.

## Acknowledgments

W. Zhang thanks Tony Lelièvre for fruitful discussions on the numerical treatment of rotational and translational invariance in the alanine dipeptide example. T. Li is supported by the NSFC under grant Nos. 11421101 and 11825102. The work of C. Schütte and W. Zhang is supported by the DFG under Germany’s Excellence Strategy-MATH+: The Berlin Mathematics Research Centre (EXC-2046/1)-project ID:390685689.

## A Proofs in Section 2

In this section, we prove Proposition 1 and Theorem 1 in Section 2.

*Proof of Proposition 1.* For any  $f \in L_0^2(\mu)$ , Lemma 1 implies that  $g = (-\mathcal{L})^{-1}f \in \mathcal{H}^1$ . Using Cauchy-Schwarz inequality and applying (16) to  $g$ , we find

$$\|g\|_1^2 = \langle g, -\mathcal{L}g \rangle_\mu \leq \|g\|_\mu \|\mathcal{L}g\|_\mu \leq \sqrt{\frac{1}{\lambda}} \langle g, (-\mathcal{L})g \rangle_\mu^{\frac{1}{2}} \|\mathcal{L}g\|_\mu = \sqrt{\frac{1}{\lambda}} \|g\|_1 \|\mathcal{L}g\|_\mu,$$

which implies that  $\|g\|_1 \leq \sqrt{\frac{1}{\lambda}} \|\mathcal{L}g\|_\mu$ , or equivalently,

$$\|(-\mathcal{L})^{-1}f\|_1 \leq \sqrt{\frac{1}{\lambda}} \|f\|_\mu, \quad \forall f \in L_0^2(\mu). \quad (58)$$

To show that the operator  $(-\mathcal{L})^{-1} : L_0^2(\mu) \rightarrow L_0^2(\mu)$  is compact (see [66, Lemma 6.9] and [58, Section VI.5] for equivalent definitions of compact operators), we consider any sequence of functions  $(f_i)_{i \geq 1}$  that are bounded in  $L_0^2(\mu)$ . Define  $g_i = (-\mathcal{L})^{-1} f_i$  for  $i \geq 1$ . The inequality (58) implies that the sequence  $(g_i)_{i \geq 1}$  is bounded in  $\mathcal{H}^1$ . Since the embedding  $\mathcal{H}^1 \hookrightarrow L_0^2(\mu)$  is compact by Lemma 1, there is a subsequence of  $(g_i)_{i \geq 1}$  which converges in  $L_0^2(\mu)$ . This shows that  $(-\mathcal{L})^{-1}$  is a compact operator.

Concerning the second item, note that the first item implies that the operator  $(-\mathcal{L} - \lambda I)^{-1}$  is compact for  $\lambda = 0$ . Applying [57, Theorem XIII.64], we know that there exists an orthonormal basis  $(\varphi_i)_{i \geq 1}$  of  $L_0^2(\mu)$ , such that  $\varphi_i \in D(\mathcal{L})$  and  $-\mathcal{L}\varphi_i = \lambda_i \varphi_i$  for  $i \geq 1$ , where  $\lambda_1 \leq \lambda_2 \leq \dots$  and  $\lim_{i \rightarrow +\infty} \lambda_i = +\infty$ . From this fact, it is not difficult to argue that the spectrum of  $-\mathcal{L}$  consists of the discrete eigenvalues  $(\lambda_i)_{i \geq 1}$ .  $\square$

*Proof of Theorem 1.* Let  $f_1, f_2, \dots, f_K \in \mathcal{H}^1$  be  $K$  functions such that (23) holds. Using the fact that  $\Sigma$  (21) is a diagonal matrix and the diagonal elements of  $F^{(K)}(f_1, f_2, \dots, f_K)$  in (20) are  $\mathcal{E}(f_1), \mathcal{E}(f_2), \dots, \mathcal{E}(f_K)$  (see (15)), we find

$$\sum_{i=1}^K \omega_i \mathcal{E}(f_i) = \text{tr}(\Sigma F^{(K)}(f_1, f_2, \dots, f_K)), \quad (59)$$

which is the second equality of (22).

Next, we show the first identity in (22). Using (20) and applying the Poincaré inequality (16), we find that

$$c^T F^{(K)}(f_1, f_2, \dots, f_K) c = \mathcal{E}\left(\sum_{i=1}^K c_i f_i\right) \geq \lambda \left\| \sum_{i=1}^K c_i f_i \right\|_{\mu}, \quad \forall c \in \mathbb{R}^K, \quad (60)$$

for some  $\lambda > 0$ . Since  $f_1, \dots, f_K$  are linearly independent due to (23), the inequality (60) implies that  $F^{(K)}(f_1, f_2, \dots, f_K)$  is positive definite, and we denote its eigenvalues as  $0 < \tilde{\lambda}_1 \leq \tilde{\lambda}_2 \leq \dots \leq \tilde{\lambda}_K$ . Applying Ruhe's trace inequality [42, H.1.h, Section H, Chapter 9], we obtain from (59) that

$$\sum_{i=1}^K \omega_i \mathcal{E}(f_i) = \text{tr}(\Sigma F^{(K)}(f_1, f_2, \dots, f_K)) \geq \sum_{i=1}^K \omega_i \tilde{\lambda}_i. \quad (61)$$

Let us show that  $\tilde{\lambda}_k \geq \lambda_k$  for  $k \in \{1, 2, \dots, K\}$ . For this purpose, applying the min-max principle for symmetric matrices gives

$$\tilde{\lambda}_k = \min_{S_k} \max_{c \in S_k, |c|=1} c^T F^{(K)}(f_1, f_2, \dots, f_K) c = \min_{S_k} \max_{c \in S_k, |c|=1} \mathcal{E}\left(\sum_{i=1}^K c_i f_i\right), \quad (62)$$

where  $S_k$  goes over all  $k$ -dimensional subspaces of  $\mathbb{R}^K$  and the second equality follows from direct calculation using (20). Since  $(f_i)_{1 \leq i \leq K} \subset \mathcal{H}^1$  satisfies

the orthonormality condition (23), each  $k$ -dimensional subspace  $S_k \subset \mathbb{R}^K$  defines a  $k$ -dimensional subspace of  $\mathcal{H}^1$  by  $\tilde{H}_k = \{ \sum_{i=1}^K c_i f_i \mid c \in S_k \}$  such that  $\tilde{H}_k \subset \text{span}\{f_1, f_2, \dots, f_K\}$ . On the contrary, every  $k$ -dimensional subspace  $\tilde{H}_k \subset \text{span}\{f_1, f_2, \dots, f_K\}$  can be written in this way for some  $k$ -dimensional subspace  $S_k \subset \mathbb{R}^K$ . Therefore, using (18), we find from (62) that

$$\tilde{\lambda}_k = \min_{S_k} \max_{c \in S_k, |c|=1} \mathcal{E}\left(\sum_{i=1}^k c_i f_i\right) = \min_{\tilde{H}_k} \max_{f \in \tilde{H}_k, \|f\|_\mu=1} \mathcal{E}(f) \geq \lambda_k. \quad (63)$$

Combining (63) and (61), gives

$$\sum_{i=1}^K \omega_i \mathcal{E}(f_i) = \text{tr}(\Sigma F^{(K)}(f_1, f_2, \dots, f_K)) \geq \sum_{i=1}^K \omega_i \tilde{\lambda}_i \geq \sum_{i=1}^K \omega_i \lambda_i.$$

Since the eigenfunctions  $(\varphi_i)_{1 \leq i \leq K}$  satisfy (23) and we have the identity  $\sum_{i=1}^K \omega_i \mathcal{E}(\varphi_i) = \sum_{i=1}^K \omega_i \lambda_i$ , we conclude that the first equality in (22) holds and the minimum is achieved when  $f_i = \varphi_i$  for  $i \in \{1, 2, \dots, K\}$ .  $\square$

## References

- [1] M. V. BALASHOV, B. T. POLYAK, AND A. A. TREMBA, *Gradient projection and conditional gradient methods for constrained nonconvex minimization*, Numer. Funct. Anal. Optim., 41 (2020), pp. 822–849, <https://doi.org/10.1080/01630563.2019.1704780>.
- [2] Z. BELKACEMI, P. GKEKA, T. LELIÈVRE, AND G. STOLTZ, *Chasing collective variables using autoencoders and biased trajectories*, (2021), <https://arxiv.org/abs/2104.11061>.
- [3] A. BOVIER AND F. DEN HOLLANDER, *Metastability: A Potential-Theoretic Approach*, Grundlehren der Mathematischen Wissenschaften, Springer International Publishing, 2015, <https://doi.org/10.1007/978-3-319-24777-9>.
- [4] C. L. BRIS, T. LELIÈVRE, M. LUSKIN, AND D. PEREZ, *A mathematical formalization of the parallel replica dynamics*, Monte Carlo Methods Appl., 18 (2012), pp. 119–146, <https://doi.org/10.1515/mcma-2012-0003>.
- [5] M. BUDIŠIĆ, R. MOHR, AND I. MEZIĆ, *Applied Koopmanism*, Chaos, 22 (2012), p. 047510, <https://doi.org/10.1063/1.4772195>.
- [6] W. CHEN AND A. L. FERGUSON, *Molecular enhanced sampling with autoencoders: On-the-fly collective variable discovery and accelerated free energy landscape exploration*, J. Comput. Chem., 39 (2018), pp. 2079–2102, <https://doi.org/10.1002/jcc.25520>.

- [7] W. CHEN, H. SIDKY, AND A. L. FERGUSON, *Nonlinear discovery of slow molecular modes using state-free reversible vampnets*, J. Chem. Phys., 150 (2019), p. 214114, <https://doi.org/10.1063/1.5092521>.
- [8] W. CHEN, A. R. TAN, AND A. L. FERGUSON, *Collective variable discovery and enhanced sampling using autoencoders: Innovations in network architecture and error function design*, J. Chem. Phys., 149 (2018), p. 072312, <https://doi.org/10.1063/1.5023804>.
- [9] J. D. CHODERA AND F. NOÉ, *Markov state models of biomolecular conformational dynamics*, Curr. Opin. Struct. Biol., 25 (2014), pp. 135–144, <https://doi.org/10.1016/j.sbi.2014.04.002>.
- [10] J. COMER, J. C. GUMBART, J. HÉNIN, T. LELIÈVRE, A. POHORILLE, AND C. CHIPOT, *The adaptive biasing force method: everything you always wanted to know but were afraid to ask*, J. Phys. Chem. B, 119 (2015), pp. 1129–1151, <https://doi.org/10.1021/jp506633n>.
- [11] E. DARVE AND A. POHORILLE, *Calculating free energies using average force*, J. Chem. Phys., 115 (2001), pp. 9169–9183, <https://doi.org/10.1063/1.1410978>.
- [12] D. DOWN, S. P. MEYN, AND R. L. TWEEDIE, *Exponential and uniform ergodicity of Markov processes*, Ann. Probab., 23 (1995), pp. 1671–1691, <https://doi.org/10.1214/aop/1176987798>.
- [13] A. B. DUNCAN, T. LELIÈVRE, AND G. PAVLIOTIS, *Variance reduction using nonreversible Langevin samplers*, J. Stat. Phys., 163 (2016), pp. 457–491, <https://doi.org/10.1007/s10955-016-1491-2>.
- [14] W. E AND B. YU, *The deep Ritz method: A deep learning-based numerical algorithm for solving variational problems*, Commun. Math. Stat., 6 (2018), pp. 1–12, <https://doi.org/10.1007/s40304-018-0127-z>.
- [15] G. FIORIN, M. L. KLEIN, AND J. HÉNIN, *Using collective variables to drive molecular dynamics simulations*, Mol. Phys., 111 (2013), pp. 3345–3362, <https://doi.org/10.1080/00268976.2013.813594>.
- [16] P. GKEKA, G. STOLTZ, A. BARATI FARIMANI, Z. BELKACEMI, M. CERIOTTI, J. D. CHODERA, A. R. DINNER, A. L. FERGUSON, J.-B. MAILLET, H. MINOUX, C. PETER, F. PIETRUCCHI, A. SILVEIRA, A. TKATCHENKO, Z. TRSTANOVA, R. WIEWIORA, AND T. LELIÈVRE, *Machine learning force fields and coarse-grained variables in molecular dynamics: Application to materials and biological systems*, J. Chem. Theory Comput., 16 (2020), pp. 4757–4775, <https://doi.org/10.1021/acs.jctc.0c00355>.

- [17] J. HAN, A. JENTZEN, AND W. E., *Solving high-dimensional partial differential equations using deep learning*, Proc. Natl. Acad. Sci. USA, 115 (2018), pp. 8505–8510, <https://doi.org/10.1073/pnas.1718942115>.
- [18] J. HAN, J. LU, AND M. ZHOU, *Solving high-dimensional eigenvalue problems using deep neural networks: A diffusion Monte Carlo like approach*, J. Comput. Phys., 423 (2020), p. 109792, <https://doi.org/10.1016/j.jcp.2020.109792>.
- [19] J. HAN, L. ZHANG, AND W. E., *Solving many-electron Schrödinger equation using deep neural networks*, J. Comput. Phys., 399 (2019), p. 108929, <https://doi.org/10.1016/j.jcp.2019.108929>.
- [20] J. HÉNIN AND C. CHIPOT, *Overcoming free energy barriers using unconstrained molecular dynamics simulations*, J. Chem. Phys., 121 (2004), pp. 2904–2914, <https://doi.org/10.1063/1.1773132>.
- [21] J. HERMANN, Z. SCHÄTZLE, AND F. NOÉ, *Deep-neural-network solution of the electronic Schrödinger equation*, Nat. Chem., 12 (2020), pp. 891–897, <https://doi.org/10.1038/s41557-020-0544-y>.
- [22] V. HERNANDEZ, J. E. ROMAN, AND V. VIDAL, *Slepc: A scalable and flexible toolkit for the solution of eigenvalue problems*, ACM Trans. Math. Softw., 31 (2005), p. 351–362, <https://doi.org/10.1145/1089014.1089019>.
- [23] B. E. HUSIC AND V. S. PANDE, *Markov state models: From an art to a science*, J. Amer. Chem. Soc., 140 (2018), pp. 2386–2396, <https://doi.org/10.1021/jacs.7b12191>.
- [24] H. JIN, M. MATTHEAKIS, AND P. PROTOPAPAS, *Physics-informed neural networks for quantum eigenvalue problems*, (2022), <https://arxiv.org/abs/2203.00451>.
- [25] W. KABSCHE, *A solution for the best rotation to relate two sets of vectors*, Acta Cryst. A, 32 (1976), pp. 922–923, <https://doi.org/10.1107/S0567739476001873>.
- [26] D. P. KINGMA AND J. BA, *Adam: A method for stochastic optimization*, in 3rd International Conference on Learning Representations, ICLR 2015, San Diego, CA, USA, May 7-9, 2015, Conference Track Proceedings, Y. Bengio and Y. LeCun, eds., 2015, <http://arxiv.org/abs/1412.6980>.
- [27] S. KLUS, P. KOLTAI, AND C. SCHÜTTE, *On the numerical approximation of the Perron-Frobenius and Koopman operator*, J. Comput. Dyn., 3 (2016), pp. 51–79.

- [28] S. KLUS, F. NÜSKE, P. KOLTAI, H. WU, I. KEVREKIDIS, C. SCHÜTTE, AND F. NOÉ, *Data-driven model reduction and transfer operator approximation*, J. Nonlinear Sci., 28 (2018), pp. 985–1010, <https://doi.org/10.1007/s00332-017-9437-7>.
- [29] I. LAGARIS, A. LIKAS, AND D. FOTIADIS, *Artificial neural network methods in quantum mechanics*, Comput. Phys. Commun., 104 (1997), pp. 1–14, [https://doi.org/10.1016/S0010-4655\(97\)00054-4](https://doi.org/10.1016/S0010-4655(97)00054-4).
- [30] A. LAIO AND F. L. GERVASIO, *Metadynamics: a method to simulate rare events and reconstruct the free energy in biophysics, chemistry and material science*, Rep. Prog. Phys., 71 (2008), p. 126601, <https://doi.org/10.1088/0034-4885/71/12/126601>.
- [31] A. LAIO AND M. PARRINELLO, *Escaping free-energy minima*, Proc. Natl. Acad. Sci. USA, 99 (2002), pp. 12562–12566, <https://doi.org/10.1073/pnas.202427399>.
- [32] J. C. LATORRE, P. METZNER, C. HARTMANN, AND C. SCHÜTTE, *A structure-preserving numerical discretization of reversible diffusions*, Commun. Math. Sci., 9 (2011), pp. 1051–1072, <https://doi.org/10.4310/CMS.2011.v9.n4.a6>.
- [33] B. J. LEIMKUHLER, T. POUCHON, T. VLAAR, AND A. J. STORKEY, *Constraint-based regularization of neural networks*, CoRR, abs/2006.10114 (2020), <https://arxiv.org/abs/2006.10114>.
- [34] T. LELIÈVRE AND G. STOLTZ, *Partial differential equations and stochastic methods in molecular dynamics*, Acta Numer., 25 (2016), pp. 681–880, <https://doi.org/10.1017/S0962492916000039>.
- [35] T. LELIÈVRE, G. STOLTZ, AND W. ZHANG, *Multiple projection MCMC algorithms on submanifolds*, (2020), <https://arxiv.org/abs/2003.09402>.
- [36] A. LESAGE, T. LELIÈVRE, G. STOLTZ, AND J. HÉNIN, *Smoothed biasing forces yield unbiased free energies with the extended-system adaptive biasing force method*, J. Phys. Chem. B, 121 (2017), pp. 3676–3685, <https://doi.org/10.1021/acs.jpcc.6b10055>.
- [37] Q. LI, B. LIN, AND W. REN, *Computing committor functions for the study of rare events using deep learning*, J. Chem. Phys., 151 (2019), p. 054112, <https://doi.org/10.1063/1.5110439>.
- [38] E. H. LIEB AND M. LOSS, *Analysis*, Graduate studies in mathematics, American Mathematical Society, 2nd ed., 2001.



- [39] J. LU AND Y. LU, *A priori generalization error analysis of two-layer neural networks for solving high dimensional Schrödinger eigenvalue problems*, (2021), <https://arxiv.org/abs/2105.01228>.
- [40] A. MARDT, L. PASQUALI, H. WU, AND F. NOÉ, *VAMPnets for deep learning of molecular kinetics*, *Nat. Commun.*, 9 (2018), <https://doi.org/10.1038/s41467-017-02388-1>.
- [41] E. MARINARI AND G. PARISI, *Simulated tempering: A new Monte Carlo scheme*, *EPL*, 19 (1992), pp. 451–458, <https://doi.org/10.1209/0295-5075/19/6/002>.
- [42] A. W. MARSHALL, I. OLKIN, AND B. C. ARNOLD, *Inequalities: Theory of Majorization and its Applications*, vol. 143, Springer, 2nd ed., 2011, <https://doi.org/10.1007/978-0-387-68276-1>.
- [43] J. MATTINGLY, A. STUART, AND D. HIGHAM, *Ergodicity for SDEs and approximations: locally Lipschitz vector fields and degenerate noise*, *Stoch. Proc. Appl.*, 101 (2002), pp. 185–232, [https://doi.org/10.1016/S0304-4149\(02\)00150-3](https://doi.org/10.1016/S0304-4149(02)00150-3).
- [44] F. NOÉ AND F. NÜSKE, *A variational approach to modeling slow processes in stochastic dynamical systems*, *Multiscale Model. Simul.*, 11 (2013), pp. 635–655, <https://doi.org/10.1137/110858616>.
- [45] F. NÜSKE, B. G. KELLER, G. PÉREZ-HERNÁNDEZ, A. MEY, AND F. NOÉ, *Variational approach to molecular kinetics*, *J. Chem. Theory Comput.*, 10 (2014), pp. 1739–1752, <https://doi.org/10.1021/ct4009156>.
- [46] N. NÜSKEN AND L. RICHTER, *Interpolating between BSDEs and PINNs – deep learning for elliptic and parabolic boundary value problems*, (2021), <https://arxiv.org/abs/2112.03749>.
- [47] B. ØKSENDAL, *Stochastic Differential Equations: An Introduction with Applications*, Springer, 5th ed., 2000.
- [48] S. OLLA, C. LANDIM, AND T. KOMOROWSKI, *Fluctuations in Markov Processes. Time Symmetry and Martingale Approximation.*, *Grundlehren der Mathematischen Wissenschaften*, Springer, 2012, <https://doi.org/10.1007/978-3-642-29880-6>.
- [49] G. PAVLIOTIS, *Stochastic Processes and Applications: Diffusion Processes, the Fokker–Planck and Langevin Equations*, Springer, 2014.
- [50] G. PÉREZ-HERNÁNDEZ, F. PAUL, T. GIORGINO, G. DE FABRITIIS, AND F. NOÉ, *Identification of slow molecular order parameters for markov model construction*, *J. Chem. Phys.*, 139 (2013), p. 015102, <https://doi.org/10.1063/1.4811489>.

- [51] B. PETERS AND B. L. TROUT, *Obtaining reaction coordinates by likelihood maximization*, J. Chem. Phys., 125 (2006), p. 054108, <https://doi.org/10.1063/1.2234477>.
- [52] P. PETERSEN AND F. VOIGTLAENDER, *Optimal approximation of piecewise smooth functions using deep ReLU neural networks*, Neural Netw., 108 (2018), pp. 296–330, <https://doi.org/10.1016/j.neunet.2018.08.019>.
- [53] D. PFAU, J. S. SPENCER, A. G. D. G. MATTHEWS, AND W. M. C. FOULKES, *Ab initio solution of the many-electron Schrödinger equation with deep neural networks*, Phys. Rev. Research, 2 (2020), p. 033429, <https://doi.org/10.1103/PhysRevResearch.2.033429>.
- [54] J. C. PHILLIPS, D. J. HARDY, J. D. C. MAIA, J. E. STONE, J. V. RIBEIRO, R. C. BERNARDI, R. BUCH, G. FIORIN, J. HÉNIN, W. JIANG, R. MCGREEVY, M. C. R. MELO, B. K. RADAK, R. D. SKEEL, A. SINGHAROY, Y. WANG, B. ROUX, A. AKSIMENTIEV, Z. LUTHEY-SCHULTEN, L. V. KALÉ, K. SCHULTEN, C. CHIPOT, AND E. TAJKHORSHID, *Scalable molecular dynamics on CPU and GPU architectures with NAMD*, J. Chem. Phys., 153 (2020), p. 044130, <https://doi.org/10.1063/5.0014475>.
- [55] J.-H. PRINZ, H. WU, M. SARICH, B. KELLER, M. SENNE, M. HELD, J. D. CHODERA, C. SCHÜTTE, AND F. NOÉ, *Markov models of molecular kinetics: Generation and validation*, J. Chem. Phys., 134 (2011), 174105, p. 174105, <https://doi.org/10.1063/1.3565032>.
- [56] C. QU, Y. LI, AND H. XU, *Non-convex conditional gradient sliding*, in Proceedings of the 35th International Conference on Machine Learning, vol. 80, PMLR, 2018, pp. 4208–4217, <http://proceedings.mlr.press/v80/qu18a.html>.
- [57] M. REED AND B. SIMON, *Methods of Modern Mathematical Physics, IV: Analysis of Operators*, Academic Press, 1978.
- [58] M. REED AND B. SIMON, *Methods of Modern Mathematical Physics, I: Functional Analysis*, Elsevier Science, 1981.
- [59] Y. M. RHEE AND V. S. PANDE, *Multiplexed-replica exchange molecular dynamics method for protein folding simulation*, Biophys. J., 84 (2003), pp. 775–786, [https://doi.org/10.1016/S0006-3495\(03\)74897-8](https://doi.org/10.1016/S0006-3495(03)74897-8).
- [60] A. RUHE, *Perturbation bounds for means of eigenvalues and invariant subspaces*, BIT Numer. Math., 10 (1970), pp. 343–354, <https://doi.org/10.1007/BF01934203>.

- [61] C. SCHÜTTE, W. HUISINGA, AND P. DEUFLHARD, *Transfer operator approach to conformational dynamics in biomolecular systems*, in Ergodic Theory, Analysis, and Efficient Simulation of Dynamical Systems, B. Fiedler, ed., 2001, pp. 191–223.
- [62] C. R. SCHWANTES AND V. S. PANDE, *Modeling molecular kinetics with tica and the kernel trick*, *J. Chem. Theory Comput.*, 11 (2015), p. 600–608, <https://doi.org/10.1021/ct5007357>.
- [63] H. SIDKY, W. CHEN, AND A. L. FERGUSON, *Machine learning for collective variable discovery and enhanced sampling in biomolecular simulation*, *Mol. Phys.*, 118 (2020), p. e1737742, <https://doi.org/10.1080/00268976.2020.1737742>.
- [64] M. M. SULTAN, G. KISS, D. SHUKLA, AND V. S. PANDE, *Automatic selection of order parameters in the analysis of large scale molecular dynamics simulations*, *J. Chem. Theory Comput.*, 10 (2014), pp. 5217–5223, <https://doi.org/10.1021/ct500353m>.
- [65] M. M. SULTAN AND V. S. PANDE, *Automated design of collective variables using supervised machine learning*, *J. Chem. Phys.*, 149 (2018), p. 094106, <https://doi.org/10.1063/1.5029972>.
- [66] G. TESCHL, *Mathematical Methods in Quantum Mechanics: With Applications to Schrödinger Operators*, Graduate studies in mathematics, American Mathematical Society, 2009.
- [67] E. VANDEN-EIJNDEN, *Transition path theory*, in Computer Simulations in Condensed Matter Systems: From Materials to Chemical Biology Volume 1, M. Ferrario, G. Ciccotti, and K. Binder, eds., vol. 703 of Lecture Notes in Physics, Springer Berlin Heidelberg, 2006, pp. 453–493.
- [68] M. O. WILLIAMS, I. G. KEVREKIDIS, AND C. W. ROWLEY, *A data-driven approximation of the Koopman operator: Extending dynamic mode decomposition*, *J. Nonlinear Sci.*, 25 (2015), pp. 1307–1346, <https://doi.org/10.1007/s00332-015-9258-5>.
- [69] H. WU AND F. NOÉ, *Variational approach for learning Markov processes from time series data*, *J. Nonlinear Sci.*, (2020), pp. 23–66, <https://doi.org/10.1007/s00332-019-09567-y>.
- [70] W. ZHANG, *Ergodic SDEs on submanifolds and related numerical sampling schemes*, *ESAIM: Math. Model. Num.*, 54 (2020), pp. 391–430, <https://doi.org/10.1051/m2an/2019071>.

- [71] W. ZHANG, C. HARTMANN, AND C. SCHÜTTE, *Effective dynamics along given reaction coordinates, and reaction rate theory*, Faraday Discuss., 195 (2016), pp. 365–394, <https://doi.org/10.1039/C6FD00147E>.
- [72] W. ZHANG AND C. SCHÜTTE, *Reliable approximation of long relaxation timescales in molecular dynamics*, Entropy, 19 (2017), <https://doi.org/10.3390/e19070367>.